bioRxiv preprint doi: https://doi.org/10.1101/2025.02.02.636139; this version posted February 6, 2025. The copyright holder for this preprint (which was not certified by peer review) is the author/funder, who has granted bioRxiv a license to display the preprint in perpetuity. It is made available under aCC-BY-NC-ND 4.0 International license.

Research Article

LRRC8A-containing anion channels promote glioblastoma proliferation via a WNK1/mTORC2-dependent mechanism

Antonio M. Fidaleo[1]*, Martin D. Bach[1]*, Shaina Orbeta[1], Iskandar F. Abdullaev[1‡], Nina Martino[2], Alejandro P. Adam[2], Mateo A. Boulos[1], Nickolai O. Dulin[4], Alexandra R. Paul[3], Yu-Hung Kuo[5], and Alexander A. Mongin[1]

[1]Department of Neuroscience and Experimental Therapeutics, [2]Department of Molecular and Cellular Physiology, and [3]Department of Neurosurgery, Albany Medical College, Albany, NY, USA

[4]Department of Medicine, Section of Pulmonary and Critical Care Medicine, The University of Chicago, Chicago, IL, USA

[5]Neurosurgery, Luminis Health Anne Arundel Medical Center, Annapolis, MD, USA

*These authors contributed equally to this work and therefore should be considered co-first authors

[‡]Current affiliation: New Uzbekistan University, Tashkent, Uzbekistan

bioRxiv preprint doi: https://doi.org/10.1101/2025.02.02.636139; this version posted February 6, 2025. The copyright holder for this preprint (which was not certified by peer review) is the author/funder, who has granted bioRxiv a license to display the preprint in perpetuity. It is made available under aCC-BY-NC-ND 4.0 International license.

SUMMARY

Leucine-rich repeat-containing protein 8A (LRRC8A) is the essential subunit of ubiquitous volume-regulated anion channels (VRACs). LRCC8A is overexpressed in several cancers and promotes negative survival outcomes via a poorly defined mechanism. Here, we explored the role of LRRC8A and VRACs in the progression of glioblastoma (GBM), the most common and deadly primary brain tumor. We found that, as compared to healthy controls, *LRRC8A* mRNA was strongly upregulated in surgical GBM specimens, patient-derived GBM cell lines, and GBM datasets from The Cancer Genome Atlas (TCGA). Our in-silico analysis indicated that patients belonging to the lowest *LRRC8A* expression quartile demonstrated a trend for extended life expectancy. In patient-derived GBM cultures, siRNA-driven LRRC8A knockdown reduced cell proliferation and additionally decreased intracellular chloride levels and inhibited activity of mTOR complex 2. The antiproliferative effect of LRRC8A downregulation was recapitulated with a pharmacological inhibitor of VRAC. Our ensuing biochemical and molecular biology analyses established that the LRRC8A-containing VRACs facilitate GBM proliferation via a new mechanism involving non-enzymatic actions of the chloride-sensitive protein kinase WNK1. Accordingly, the chloride-bound WNK1 stimulates mTORC2 and the mTORC2-dependent protein kinases AKT and SGK, which promote proliferation. These findings establish the new mTORC2-centric axis for VRAC dependent regulation of cellular functions and uncover potential targets for GBM intervention.

SUBJECT AREAS

Cell biology

Molecular biology

Cancer

bioRxiv preprint doi: https://doi.org/10.1101/2025.02.02.636139; this version posted February 6, 2025. The copyright holder for this preprint (which was not certified by peer review) is the author/funder, who has granted bioRxiv a license to display the preprint in perpetuity. It is made available under aCC-BY-NC-ND 4.0 International license.

INTRODUCTION

Glioblastoma (GBM) is the most common and aggressive primary brain cancer in adults that arises due to the accumulation of somatic mutations in neural or glial precursor cells.[1,2,3] With an annual incidence rate of ~3.2 cases per 100,000 people, GBM accounts for approximately half of all primary brain malignancies.[4] Compared to other brain tumors, GBM is associated with disproportionately high morbidity and mortality, with the majority of patients dying within two years of diagnosis and only 5-6% surviving past five years.[4,5] Based on extensive clinical evidence, the standard of care for GBM patients includes maximal safe tumor resection followed by radio- and chemotherapy with the brain-penetrable alkylating agent temozolomide.[6,7,8] Unfortunately, the highly infiltrative nature of GBM makes complete removal nearly impossible; furthermore, GBM tumors rapidly develop resistance to the first-line therapies and invariantly recur. [5,7,8] Even the most aggressive treatment regiments increase median survival time only marginally and do not extend median life expectancy past 15-16 months.[5,7] The inherent resistance of GBMs to all current treatment modalities, alongside the high degree of intertumoral and intratumoral heterogeneity, necessitates the search for new prospective therapeutic targets. Some of the recently developed and tested approaches include tumor-treating fields[9], viral and immune therapies (e.g.,[10,11,12]), and inhibitors of signaling pathways associated with GBM progression (e.g.,[13,14]).

Cancer development is frequently associated with profound changes in the expression and/or activity of ion channels, leading to the idea that cancerogenesis may be viewed as an 'onco-channelopathy' (see[15,16], and overview in[17]). Modified ion channel function has been linked to many cancer hallmarks, including unrestricted proliferation, tissue invasion, metastasis, pathological angiogenesis, and evasion of apoptosis (reviewed in[15,16,18,19,20,21,22]). Chloride (Cl^-) channels are a diverse group of membrane proteins which facilitate movement of Cl^-, bicarbonate, and various small organic molecules. They regulate numerous cellular processes, including many of those relevant to cancer biology. [23,24,25] Among many distinct Cl^- channels, volume regulated anion channels (VRACs) have long been speculated to contribute to cancer progression[26,27], including in GBM[28,29,30]. The ubiquitous VRACs, also known as volume-sensitive organic osmolyte-anion channels (VSOAC) or volume-sensitive outward rectifying chloride channels (VSOR), are activated by cell swelling and are the key players in cell volume regulation.[26,31,32]. However, they are also thought to be important for cell proliferation, migration, angiogenesis, apoptotic cell death, and chemoresistance.[22,26,33,34,35]

For a long time, progress in VRAC research was impeded by a lack of knowledge regarding the channel's molecular composition.[36] This problem persisted until about ten years ago, when two seminal studies discovered that VRACs are hexameric complexes composed of proteins from the leucine-rich repeat-containing family 8 (LRRC8), with one of these, LRRC8A, playing an indispensable role in channel function.[37,38] These new findings rapidly revolutionized the field and dramatically expanded our understanding of the physiological importance of VRACs. Thus, it was demonstrated that LRRC8A can serve as both a subunit of VRAC and as a signaling scaffold for several proteins linked to growth factor signaling.[39,40,41,42] Using a conditional deletion of the essential LRRC8A, VRACs were shown to contribute to many diverse physiological processes such as glucose sensing and metabolic regulation, fertility, paracrine signaling, immune function, and others.[40,43,44,45] Among important recent developments, several laboratories discovered that LRRC8A is upregulated in a variety of cancers and that its expression levels are inversely related to patients' life expectancy (e.g.,[46,47,48,49]). Our group was

bioRxiv preprint doi: https://doi.org/10.1101/2025.02.02.636139; this version posted February 6, 2025. The copyright holder for this preprint (which was not certified by peer review) is the author/funder, who has granted bioRxiv a license to display the preprint in perpetuity. It is made available under aCC-BY-NC-ND 4.0 International license.

the first to find that LRRC8A-containing VRACs regulate GBM proliferation and sensitivity to the chemotherapeutic agent temozolomide.[50] Here, we performed an extensive analysis of LRRC8A expression and function in human GBM and explored the intracellular mechanisms linking VRAC activity to enhanced proliferation in patient-derived GBM cells. We discovered a previously unknown Cl^- dependent mTOR complex 2-centric mechanism linking VRAC activity to cancer cell proliferation.

bioRxiv preprint doi: https://doi.org/10.1101/2025.02.02.636139; this version posted February 6, 2025. The copyright holder for this preprint (which was not certified by peer review) is the author/funder, who has granted bioRxiv a license to display the preprint in perpetuity. It is made available under aCC-BY-NC-ND 4.0 International license.

RESULTS

LRRC8A expression is upregulated in GBM tumor tissue and in patient-derived GBM cells

Based on our previous discovery of the potentially important role of LRRC8A in GBM proliferation[50], we analyzed expression levels for each of the five LRRC8 family members in surgically resected GBM specimens. We employed a qRT-PCR approach to compare 22 GBM samples to three separate brain tissue RNA medleys isolated postmortem from healthy brains and representing a total of 8 individuals (see *Star★Methods* for details). The main finding of this comparison was the dramatic upregulation of LRRC8A expression in the majority of GBM specimens which, on average, was six-times higher than in non-pathological brain tissue (Figure 1A1, $p<0.001$). In contrast, LRRC8B, LRRC8C, and LRRC8D gene products were present in comparable quantities in both malignant and non-malignant brain samples (Figure 1A1). Consistent with other reports and prior RNA-seq analyses of brain cells (see[51]), LRRC8E expression was either extremely low or undetectable (not shown). The abundance of LRRC8A mRNA in GBM was much higher than that of other LRRC8 isoforms, which is unusual when compared to the LRRC8 expression patterns in non-malignant tissues (see *Discussion*).

Keeping in mind the heterogeneity of tumor material, which contains vasculature and large numbers of invading immune cells, we extended qRT-PCR analysis of LRRC8/VRAC expression to primary GBM cell cultures derived from the surgical specimens. In these experiments, expression was compared to primary human astrocytes cultivated under identical conditions. Similar to GBM tissue data, we found that LRRC8A mRNA expression was significantly elevated, approximately five-fold, as compared to non-malignant astrocytes (Figure 1A2, $p<0.05$). Interestingly, we found that GBM cultures also had higher expression of LRRC8B, LRRC8C and LRRC8D subunits (Figure 1A2, adjusted $p<0.05$ for all transcripts). Still, the pattern of overabundance of LRRC8A mRNA relative to the other members of LRRC8 family strongly resembled that seen in surgical GBM specimens.

For independent validation of our findings, we evaluated clinical RNA-seq data available through The Cancer Genome Atlas (TCGA) program. We selected the TCGA GBM datasets that included full RNA-seq and survival information and were confirmed as expressing wild type IDH1/2 transcript. The patients with mutated IDH1/2 were excluded, as this mutation is indicative of the biologically distinct secondary GBM.[52] The transcript abundance of LRRC8 isoforms was compared between 126 primary GBMs and 3 RNA medleys representing 29 healthy brains. The healthy brain data were sourced from the Gene Expression Omnibus repository (GEO series GSE196695, see[53]). In our in-silico RNA-seq analysis, the pattern of LRRC8 subunit expression largely mirrored what was seen in our internally obtained GBM specimens. LRRC8A was by far the most prominently expressed subunit, with the median expression in GBM samples approximately 3-fold higher than in healthy brains (Figure 1A3, $p<0.001$). LRRC8B through D were expressed at much lower levels than LRRC8A, in quantities comparable across GBM and healthy brain tissue (Figure 1A3). LRRC8E was consistently low-to-undetectable throughout all datasets (not shown).

Overall, the pattern of elevated expression of LRRC8A in GBM was remarkably similar in all three analyses. In contrast, LRRC8B-D subunits were expressed in comparable quantities in malignant tissue and healthy brains.

bioRxiv preprint doi: https://doi.org/10.1101/2025.02.02.636139; this version posted February 6, 2025. The copyright holder for this preprint (which was not certified by peer review) is the author/funder, who has granted bioRxiv a license to display the preprint in perpetuity. It is made available under aCC-BY-NC-ND 4.0 International license.

LRRC8A-containing VRACs are expressed in patient-derived GBM cells and are important for GBM proliferation

Next, we assessed the functional expression and physiological relevance of LRRC8A-containing VRACs in patient-derived GBM cells. To account for intertumoral heterogeneity, we performed our in-vitro analyses in two different GBM cell lines, here referred to as GBM1 and GBM8. Both were isolated and propagated from clinically diagnosed GBM specimens but had distinct morphological and molecular features. GBM1 cells had a dedifferentiated morphology (Figure 1B and Figure S1A), very high proliferative capacity, and low-to-undetectable GFAP expression (Figure S1C). In contrast, GBM8 had an epithelial morphology resembling that of cultured astrocytes (Figure 1B and Figure S1B), lower rate of proliferation, and high expression of the astrocytic marker GFAP (Figure S1C). Consistent with their astroglial lineage, GBM1 and GBM8 had high glutamate uptake rates comparable to human astrocytes (Figure S1E-G). qRT-PCR analysis revealed moderate differences in the levels of LRRC8A mRNA expression between two primary cell lines. In GBM1, LRRC8A mRNA levels were similar to those in human astrocytes, while GBM8 had 2-4-fold higher LRRC8A mRNA abundance (Figure S1D).

To measure VRAC activity, we used a radiotracer assay quantifying swelling-activated release of the VRAC-permeable, nonmetabolizable glutamate analogue D-[^{3}H]aspartate. This method enables characterization of VRAC behavior in large cell populations and is highly suitable for cells of glial origin due to their high glutamate uptake capacity.[54,55] Application of hypoosmotic medium, which causes cell swelling, produced a strong increase in D-[^{3}H]aspartate efflux (Figure 1C) which resembled the VRAC-mediated glutamate release seen in rodent (e.g.,[54,55,56,57]) and human astrocytes (Figure 1C). The ranking of maximal release rates was GBM8 > astrocytes ≈ GBM1 (Figure 1C). Despite similarities to astrocytes, the kinetics of D-[^{3}H]aspartate release in GBM had several unique features. In GBM1, maximal hypoosmotic activation occurred 3-4 min later than in GBM8 or astrocytes, indicating slower rate of cellular swelling or difference in VRAC activation kinetics (Figure 1C). In GBM8, basal (non-stimulated) release rate was approximately 3-fold higher than in GBM1 or astrocytes, likely pointing to elevated tonic VRAC activity in non-swollen GBM8 cells (Figure 1C). These differences aside, all GBM cells demonstrated functional VRAC activity.

To confirm that VRAC activity in GBM is reliant on LRRC8A, we utilized an RNAi approach. We first probed the effectiveness of four different LRRC8A-specific siRNA constructs using qRT-PCR (Figure S2A). Two effective constructs (dubbed “siA3” and “siA5”) were further validated at the protein level using Western blotting. By day 4 post-transfection, both siA3 and siA5 reduced LRRC8A protein content by >95% in both GBM1 and GBM8 (Figure 1D). These siRNAs were then tested in VRAC activity assays. In GBM1, as compared to the negative control siNC, siA3 and siA5 reduced swelling-activated D-[^{3}H]aspartate release via VRAC by ≥80% (Figure 1E, Figure S2C). Strong inhibition of VRAC activity by LRRC8A siRNA was also observed in GBM8 (Figure S2D). Altogether, these results suggest that LRRC8A protein is essential for VRAC function in GBM and can be effectively downregulated by employing RNAi.

Using RNAi, we further explored the impact of LRRC8A knockdown on GBM proliferation measured as cumulative changes in cell numbers over 96 h after siRNA transfection. In MTT assays, the LRRC8A siRNAs, siA3 and siA5, reduced cell numbers by 50-55% in GBM1 and 25-35% in GBM8 (Figure 1F). MTT results were independently confirmed using automated counting of DAPI-stained GBM nuclei. The LRRC8A-specific siA3 and siA5 strongly reduced the numbers of substrate-attached GBM1 and GBM8 cells (Figure S3). In our prior work[50], we

bioRxiv preprint doi: https://doi.org/10.1101/2025.02.02.636139; this version posted February 6, 2025. The copyright holder for this preprint (which was not certified by peer review) is the author/funder, who has granted bioRxiv a license to display the preprint in perpetuity. It is made available under aCC-BY-NC-ND 4.0 International license.

additionally cross-validated the effects of LRRC8A knockdown on proliferation by physically counting GBM cells using a Coulter counter. Potential contributions of cell death to the differences in cell numbers were ruled out because we found no significant increase in lactate dehydrogenase release from cells treated with siA3 or siA5 (Figure S4). As a positive control, treatment with 300 nM staurosporine caused ~50% cell death within 24 h (Figure S4). Altogether, these results strongly support the notion that elevated LRRC8A expression in GBM boosts high rates of cell proliferation.

The relationship between LRRC8A expression and clinical GBM outcomes

High expression of LRRC8A has been putatively linked to shorter life expectancy in several cancers (e.g.,[46,47,48,49]). Therefore, we analyzed if tumoral *Lrrc8a* mRNA levels in primary GBM correlate with clinical outcomes by performing survival analysis in TCGA datasets. The LRRC8A expression data presented in Figure 1A3 were additionally normalized using the DEseq2 variance-stabilizing transformation.[58] This type of normalization is considered superior because it accounts for sample-to-sample differences in library size, sequencing depth, false positives, etc.[59,60] 126 GBM TCGA patients were divided into quartiles based on their tumor *Lrrc8a* mRNA expression (Figure 2A) and analyzed for differences in their life expectancy (Figure 2B). We found that patients with the lowest *Lrrc8a* expression (Q1) had a median survival time of 480 days, which was 120+ days longer than the median survival in Q2 (333 days), Q3 (360 days), and Q4 (360 days) (Figure 2B), denoting a 33% increase in patient life expectancy. Considering the close clustering of expression levels in Q2 and Q3, we statistically compared only the highest (Q4) and the lowest (Q1) LRRC8A expression quartiles and found a trend for longer survival in Q1 (Gehan-Breslow-Wilcoxon test, p=0.078). Superficially, these results are consistent with the proliferation-promoting role for LRRC8A. However, the overall correlation between LRRC8A expression levels and survival appears to be weak, and its significance remains unclear.

Lack of consistent effect of LRRC8A knockdown on cell cycle or cell-cycle dependent proteins

Although LRRC8A expression has been linked to high proliferative rates in several cancers (see[50,46,47,48,49]), the underlying mechanisms are far from clear and may be cancer specific. To further explore the role of LRRC8A in GBM proliferation, we started with an analysis of cell cycle progression using fluorescence-activated cell sorting (FACS) of propidium iodide-stained cells. We found significant differences between GBM1 and GBM8 cells in terms of their allocation among various cell cycle phases. In non-synchronized cultures of GBM1, ~80%, ~3%, and ~10% of cells were found in G_1/G_0, S, and G_2/M stages of mitotic cycle, respectively (Figure S5A,C, the remaining cells were polyploid). GBM8 demonstrated a different cell cycle distribution pattern with ~60%, ~4%, and ~23% cells in G_1/G_0, S, and G_2/M mitosis phases, respectively (Figure S5, the remaining cells were polyploid). Using this approach, we found no statistical differences in the apparent mitotic progression of siNC-, siA3-, or siA5-treated cells, except for a small reduction in S phase numbers in GBM8 (Figure S5B,C). The observed lack of effect of LRRC8A knockdowns on cell cycle distribution was unexpected because of the significant reduction in cell numbers seen in LRRC8A siRNA-treated cells (compare Figure S5 to the results in Figure 1F).

bioRxiv preprint doi: https://doi.org/10.1101/2025.02.02.636139; this version posted February 6, 2025. The copyright holder for this preprint (which was not certified by peer review) is the author/funder, who has granted bioRxiv a license to display the preprint in perpetuity. It is made available under aCC-BY-NC-ND 4.0 International license.

As a complementary approach, we evaluated the expression of cell cycle-dependent proteins using Western blotting. In specific, we analyzed expression levels for cyclin D1 and its partner CDK4, and cyclin E1 and its partner CDK2. Although we found several effects of siRNA on individual cell cycle proteins (Figure S6), we identified no common pattern of effects of LRRC8A knockdown across two different siRNA species (siA3 and siA5) and two GBM cell lines (GBM1 and GBM8). Overall, the two performed cell cycle analyses provided no clear mechanistic insight into the reduction of cell proliferation seen following LRRC8A knockdown.

LRRC8A knockdown does not modify GRB2-dependent growth signaling

As a potential alternative mechanism underlying the observed changes in cell proliferation, we explored the effects of LRRC8A knockdown on growth signaling pathways. Previous work identified a physical interaction between LRRC8A and the growth factor signaling adaptor proteins GRB2 and GAB2.[39,42,61] Furthermore, ablation of LRRC8A expression has been shown to reduce enzymatic activity in a diverse range of GRB2-dependent signaling cascades.[39,42,41] Here, we focused our attention on the ERK1/2 and the JNK signaling axes, which are activated by numerous growth factor receptors and synergistically modulate AP-1 dependent gene transcription (see[62] and diagrams in Figure 3A, F). In the case of ERK1/2 signaling, GRB2 interacts with the guanine exchange factor SOS to initiate the classical Ras→Raf→MEK1/2→ Erk1/2 signal transduction ([62,63] and Figure 3A). In the case of JNK signaling, the activation may involve the GRB2-driven Ras-Rac interactions[64], or the PI3K-dependendent activation of a distinct SOS adaptor complex[65] (Figure 3F). Additionally, we explored changes in the activity of the PI3K-AKT-mTOR signaling arm, which is also activated by growth factors in a GRB2/GAB2-dependent manner and is highly relevant to malignant cell proliferation, including in GBM (see [66,67] and diagram in Figure 4A).

In GBM1, treatment with the LRRC8A-specific siA3 and siA5 produced no effect on phospho-Erk1/2 levels (p-Thr^{202}/Tyr^{204}, Figure 3B), total Erk1/2 immunoreactivity (Figure 3C), or phospho/ total Erk1/2 immunoreactivity ratio (Figure 3D). As controls, we used two inhibitors of upstream MEK1/2 kinases, U0126[68] and trametinib[69], both of which dramatically reduced Erk1/2 phospho-rylation (Figure 3B,C,E). Surprisingly, U0126 (Figure 3D) had no significant effect on the proliferation of either GBM1 or GBM8, while trametinib produced marginal inhibition (Figure S7, 12% decrease, $p<0.001$). Together, these results rule out Erk1/2 signaling as the major mechanism contributing to the effect of LRRC8A on GBM proliferation.

In the next set of experiments, we analyzed the AP-1 linked JNK signaling axis by probing phosphorylation of the canonical JNK target cJun. LRRC8A knockdowns yielded no consistent effect on phospho-cJun (p-Ser^{73}, Figure 3G), total cJun (Figure 3H), or phospho/total cJun immunoreactivity ratio (Figure 3J). As controls, we utilized the pharmacological inhibitors SP600125[70] and BSJ-04-122[71], which block JNK or the upstream kinases MKK4/7, respectively. To activate JNK, we treated cells with anisomycin. All pharmacological controls eliminated or upregulated cJun phosphorylation in the predicted manner (Figure 3G,H,J). To test the relevance of JNK signaling to GBM growth, we explored the effect of the JNK inhibitor SP600125 on GBM proliferation. Consistent with prior reports[72,73], inhibition of JNK strongly reduced GBM cell proliferation, by 55% and 38% in GBM1 and GBM8, respectively ($p<0.001$, Figure 3I). This effect was quantitatively similar to the effects of LRRC8A siRNA. However, since

bioRxiv preprint doi: https://doi.org/10.1101/2025.02.02.636139; this version posted February 6, 2025. The copyright holder for this preprint (which was not certified by peer review) is the author/funder, who has granted bioRxiv a license to display the preprint in perpetuity. It is made available under aCC-BY-NC-ND 4.0 International license.

LRRC8A knockdown caused no reduction in cJun phosphorylation, JNK signaling cannot be responsible for the pro-proliferative actions of LRRC8A.

To test for the involvement of the PI3K-AKT-mTOR pathway, we measured phosphorylation levels of one of the terminal substrates of mTORC1/S6K signaling, the ribosomal protein S6.[74] LRRC8A knockdown yielded no effect on the levels of phospho-S6 (p-Ser$^{240/244}$, Figure 4B), total S6 (Figure 4C), or the ratio of phospho-to-total S6 immunoreactivity (Figure 4E). As a control, we used the mTOR inhibitor rapamycin[75], which at low nanomolar concentrations preferentially inhibits mTORC1, and the dual mTORC1/mTORC2 blocker KU-0063794[76]. Both agents effectively reduced S6 phosphorylation by 85-95% (Figure 4B,E) confirming the specificity and the sensitivity of this assay. Finally, we tested the effect of the PI3K inhibitor PI 828[77] on GBM proliferation. This agent reduced GBM1 and GBM8 cell numbers by 28% and 19%, respectively (Figure 4D). In summary, the lack of effect of LRRC8A siRNA on phospho-S6 levels rules out the PI3K-dependent mTORC1 signaling as the basis for pro-proliferative actions of LRRC8A in GBM.

LRRC8A knockdown reduces $[Cl^-]_i$ and modifies the Cl^--sensitive WNK-SPAK/OSR1 axis

As the next alternative, we explored if GBM proliferation is regulated by VRAC-mediated Cl^- fluxes and/or changes in intracellular Cl^- levels ($[Cl^-]_i$). The activity of several Cl^- channels and the associated changes in $[Cl^-]_i$ have been linked to progression through the mitotic cycle and cell migration, including in GBM cell lines.[78,79] We first assessed $[Cl^-]_i$ in GBM by non-invasively measuring steady-state distribution of the radiotracer $^{36}Cl^-$ (see *Star★Methods* and ref.[80,81] for implementation in various cell types). In GBM1, $^{36}Cl^-$ uptake reached equilibrium within ~10 min (Figure 5A). Therefore, all subsequent experiments determined steady-state $^{36}Cl^-$ content after 20 min of incubation with this radiotracer. Using this approach, we found that LRRC8A knockdown reduced $[Cl^-]_i$ by 5-8% (Figure 5B). Although small, this effect was significant and consistent among two different siRNA constructs (8% for siA3 and 5% for siA5, $p<0.0001$ and $p<0.01$, respectively, Figure 5B). Thus, activity of the LRRC8A-containing VRACs appear to sustain high $[Cl^-]_i$. To further explore if VRAC activity modifies GBM proliferation rate, we tested the putative VRAC blocker DIDS.[82,83] The advantage of DIDS is that it is non-toxic in longitudinal cell proliferation experiments, unlike DCPIB[84]. Within a 72-h incubation period, DIDS reduced GBM1 proliferation by 49% ($p<0.001$) and GBM8 proliferation by 22% ($p=0.019$), respectively (Figure 5C). The lower efficacy in GBM8 is likely due to limited inhibition of VRAC (23% inhibition of channel activity, $p=0.015$, Figure S8). DIDS blocks VRAC poorly at negative voltages and may be less efficacious in cells with highly negative membrane potential.[82,83] With this caveat notwithstanding, our pharmacological data support the notion that VRAC modulates GBM proliferation.

Since $[Cl^-]_i$ is inversely related to the activity of the Cl^--sensitive WNK kinases and their downstream targets SPAK and OSR1[85], we further investigated if LRRC8A knockdown modulates WNK signaling. WNK activity was determined by measuring phosphorylation levels of the downstream target SPAK (p-Ser^{373}), with the caveat that the antibody used in this analysis additionally recognizes phosphorylation of the structurally and functionally homologous OSR1 (p-Ser^{325}). The LRRC8A-targeting siA3 and siA5 constructs reduced levels of phosphorylated SPAK/OSR1, by 40% ($p=0.002$) and 26% ($p=0.077$) respectively (Figure 5D). The effect was mirrored by the loss of immunoreactivity for total SPAK protein (a decrease of 46% by siA3,

bioRxiv preprint doi: https://doi.org/10.1101/2025.02.02.636139; this version posted February 6, 2025. The copyright holder for this preprint (which was not certified by peer review) is the author/funder, who has granted bioRxiv a license to display the preprint in perpetuity. It is made available under aCC-BY-NC-ND 4.0 International license.

p=0.015, and 40% by siA5, p=0.047, Figure 5E) resulting in an unchanged phospho-SPAK/total SPAK ratio (Figure 5F). The specificity of immunoblotting signals was further validated by measuring the effects of a WNK inhibitor and WNK activator. The pan-WNK inhibitor WNK463 eliminated SPAK/OSR1 phosphorylation (Figure 5D, p<0.001). Conversely, activation of WNKs by incubation in 600 mOsm hyperosmotic medium[86] increased phospho-SPAK/OSR1 signal (+52%, p<0.001, Figure 5D) and phospho/total SPAK immunoreactivity ratio (+83%, p=0.015, Figure 5F). The intermediate conclusion from these results is that LRRC8A knockdown reduces total SPAK (and likely OSR1) levels without impacting relative WNK-SPAK/OSR1 activity.

The non-enzymatic contributions of WNK1 to mTORC2 signaling and GBM proliferation

Since LRRC8A knockdown reduced SPAK expression, we further investigated if modified WNK-SPAK/OSR1 signaling might underlie the observed changes in GBM proliferation. Such an idea is consistent with prior literature reports on the important role of WNKs, including WNK1, in cell proliferation and numerous aspects of cancerogenesis (reviewed in[87,88]). We first checked if pharmacological inhibition of WNK suppresses GBM growth. The pan-inhibitor of WNK isozymes, WNK463[89], eliminated phosphorylation of downstream SPAK and OSR1 at 1 µM (Figure 5D,G) but was completely ineffective in reducing GBM proliferation across a broad concentration range of 0.1-3 µM (Figure 6A). Still, several alternative, non-enzymatic, non-SPAK/OSR1-dependent mechanisms have been proposed for WNK1 including regulation of mitotic division[90] and regulation of the pro-growth SGK1 signaling[91,92]. Therefore, we tested the effects of WNK1 knockdown using three different siRNA constructs (Figure 6B). The WNK1-targeting siRNAs reduced proliferation in both GBM1 and GBM8, in a manner that was commensurate with their effect on WNK1 mRNA expression (Figure 6C, compare to siRNA potencies in Figure 6B). The most effective WNK1 siRNA construct, termed #5, inhibited GBM1 and GBM8 proliferation by 70% and 47%, respectively (p<0.001, Figure 6C) exceeding the anti-proliferative effects of LRRC8A knockdown.

As the potent WNK inhibitor WNK463 did not affect cell proliferation (see Figure 6A), we probed for the potential involvement of a newly discovered mechanism which involves the formation of a complex between the enzymatically inactive, Cl^--bound WNK1 and mTOR complex 2 (mTORC2).[92] mTORC2 activity was assessed by measuring the phosphorylation levels of one of its substrates, AKT (phospho-Ser^{473}).[93] Two efficacious WNK1 siRNAs, construct #5 and construct #6, decreased the mTORC2-dependent phosphorylation of AKT by 74% (p<0.001) and 31% (p<0.001), respectively, in a manner that was proportional to their effect on WNK1 mRNA levels (compare to Figure 6B). There was no effect on total AKT levels (Figure 6F). Accordingly, changes in the phospho/total AKT immunoreactivity ratio (Figure 6G) mirrored the pattern of changes in phospho-AKT. As a positive control, we used the AKT inhibitor MK-2206[94], which abolished AKT phosphorylation (p<0.001, Figure 6E, G).

To test if the same signaling changes occurred following LRRC8A knockdown, we quantified levels of AKT phosphorylation in LRRC8A siRNA-treated GBM1 cells. The LRRC8A-targeting siA3 and siA5 constructs both reduced mTORC2-dependent phospho-AKT immunoreactivity, by 59% (p<0.001) and 45% (p=0.003) respectively (Figure 6H, J). There were no changes in total AKT expression levels (Figure 6I). As controls, we employed the PI3K inhibitor PI 828 and the AKT inhibitor MK-2206. Both agents eliminated AKT phosphorylation (95+% reduction in phospho-signal) without affecting total AKT levels (Figure 6H-I). Together, these results strongly

bioRxiv preprint doi: https://doi.org/10.1101/2025.02.02.636139; this version posted February 6, 2025. The copyright holder for this preprint (which was not certified by peer review) is the author/funder, who has granted bioRxiv a license to display the preprint in perpetuity. It is made available under aCC-BY-NC-ND 4.0 International license.

suggest that LRRC8A protein expression and/or VRAC function strongly modulate the activity of mTORC2.

mTORC2 signaling drives GBM proliferation

To test the plausibility of the notion that decreased mTORC2 signaling is what causes impaired proliferation in LRRC8A knockdown cells, we measured the impact of mTORC2 signaling on GBM proliferation, first by blocking mTOR activity with the mTORC1/2 inhibitor, KU-0063794.[76] This compound potently reduced proliferation of GBM1 and GBM8 by 58% ($p<0.001$) and 45% ($p<0.001$), respectively (Figure 7A, B). We next tested the effects of pharmacological inhibitors targeting the three canonical substrates of mTORC2 catalytic activity: AKT (MK-2206), SGK (GSK650394)[95], and conventional PKCα/β/γ (cPKC, Gö6976). These AGC family protein kinases are known to promote proliferation in numerous cell types (e.g.,[96]). When used individually, the AKT and SGK blockers inhibited cell growth in the range of 10-30% in both patient-derived cell lines (Figure 7A, B, $p<0.001$). The cPKC inhibitor was completely ineffective (Figure 7A, B). However, when all three agents were combined, proliferation was reduced by 53% and 42% in GBM1 and GBM8, respectively (Figure 7A, B, $p<0.001$). The apparent additive action of AKT and SGK inhibitors closely matched the effects of the mTOR blocker KU-0063794 in both GBM cell lines (Figure 7A, B). Collectively, the results of our siRNA and pharmacological experiments support the hypothesis that LRRC8A regulates GBM proliferation through activation of the mTORC2 signaling axis.

bioRxiv preprint doi: https://doi.org/10.1101/2025.02.02.636139; this version posted February 6, 2025. The copyright holder for this preprint (which was not certified by peer review) is the author/funder, who has granted bioRxiv a license to display the preprint in perpetuity. It is made available under aCC-BY-NC-ND 4.0 International license.

DISCUSSION

Three major findings of this study can be summarized as follows: (i) The Cl^- channel-forming protein LRRC8A shows a pattern of strongly elevated expression in human GBMs. (ii) RNAi analysis in patient-derived GBM cultures indicates that LRRC8A facilitates cell proliferation. (iii) the influence of LRRC8A on proliferation is mediated by a novel Cl^--sensitive signaling mechanism involving a non-enzymatic function of WNK1 and its impact on downstream mTORC2 signaling. We believe that the results reported here will be of significant interest to neuro-oncologists, as well as to the broader community of cell physiologists exploring the diverse functions of volume-regulated anion channels and the VRAC-constituting LRRC8 proteins.

This study is the first to report that LRRC8A is overexpressed in the majority of primary GBMs as compared to healthy brain tissue. The pattern of strongly elevated LRRC8A expression was consistently identified in surgical GBM specimens, patient-derived GBM cultures, and in the GBM datasets deposited in TCGA. These findings may suggest a pathological role for LRRC8A in GBM progression, with potential implications for clinical outcomes. Similar to our current work, elevated LRRC8A expression, compared to adjacent non-cancerous tissues, has been found in colon cancer, esophageal squamous cell carcinoma, hepatocellular carcinoma, gastric cancer, and pancreatic adenocarcinoma.[46,47,48,97,98] In all of these carcinomas, as well as in head-and-neck cancer, elevated LRRC8A expression was predictive of poor survival outcomes, suggesting that it may serve as a biomarker for aggressive tumors.[46,47,48,97,98,99] In contrast, in a systematic analysis of TCGA datasets, Carpanese et al. identified the opposite trend in kidney renal clear cell carcinoma, low-grade gliomas, and sarcomas, where high LRRC8A levels were associated with better survival outcomes.[99] In GBM, we found a weak correlation between LRRC8A expression and patients' life expectancy, with a trend for longer survival in the patient cohort with the lowest LRRC8A levels. Nevertheless, our data suggest that LRRC8A protein is necessary for the effective proliferation of GBM cells. This reliance on LRRC8A was confirmed in patient-derived GBM cells expressing either low (GBM1) or high (GBM8) levels of LRRC8A. We acknowledge that the dependence on LRRC8A is likely a cell type-specific phenomenon since LRRC8A deletion yielded no effect on proliferation in several non-malignant and malignant cell lines (e.g.,[100]).

Across the existing literature, no unifying mechanism for LRRC8A-dependent cancer growth has been agreed upon. Pioneer work in immune cells revealed a physical interaction between LRRC8A, GRB2, and GAB2.[39] These two scaffolding proteins transduce growth factor and cytokine receptor signaling and are critical for normal development, as well as for the proliferation and motility of cancer cells.[101,102,66] Deletion or knockdown of LRRC8A has been shown to reduce enzymatic activity in the growth factor-dependent ERK1/2 and PI3K-AKT signaling pathways in thymocytes, myocytes, endothelial cells, and other diverse cell types.[39,41,42] In our hands, LRRC8A knockdown did not cause changes in the activity of three GRB2-dependent signaling arms, namely ERK1/2, JNK, and PI3K-AKT-mTORC1. Consistent with our data in GBM, LRRC8A downregulation in hepatocellular carcinoma did not reduce relative activity of ERK1/2 or AKT.[47] Thus, regulation of GRB2-dependent signaling by LRRC8A appears to be a cell type-specific phenomenon that must be tested and confirmed on a case-by-case basis. Among other suggested mechanisms, several groups have reported that LRRC8A depletion causes disruptions in cell cycle-related signaling, such as upregulation of the CDK inhibitors $p21^{Cip1}$ and $p27^{Kip1}$ or downregulation of cyclin D1 and CDK2, in addition to increased

bioRxiv preprint doi: https://doi.org/10.1101/2025.02.02.636139; this version posted February 6, 2025. The copyright holder for this preprint (which was not certified by peer review) is the author/funder, who has granted bioRxiv a license to display the preprint in perpetuity. It is made available under aCC-BY-NC-ND 4.0 International license.

pro-apoptotic signaling and cell death.[46,47,48] In our study, despite the strong reduction in GBM cell numbers, LRRC8A knockdown did not produce consistent changes in cell cycle distribution, levels of cell cycle-related proteins, or increased apoptosis. These findings are mirrored by a recently published extensive analysis of the effect of LRRC8A knockout in colorectal carcinoma HCT116 cells, where a strong reduction in cell proliferation was not associated with changes in cell cycle distribution or apoptosis.[99] Overall, the mechanistic link between LRRC8A and cell proliferation remains obscure.

In search of an alternative explanation, we explored the impact of reduced VRAC channel activity on $[Cl^-]_i$ homeostasis. Over years, many laboratories have found that structurally diverse VRAC blockers inhibit proliferation in various cell types, including GBM (e.g.,[28,33,103,104] and reviews[26,27,105]). However, exceptions do exist.[100] For example, in C2C12 myoblasts neither pharmacological inhibition of VRAC or LRRC8A knockdown impair cell growth, but instead potently inhibit cell differentiation.[106] In our hands, the putative VRAC blocker DIDS has reduced GBM1 and GBM8 proliferation with the inhibitory potency resembling that of LRRC8A knockdown (GBM1>GBM8). The similarity of our pharmacology and molecular biology results, combined with existing published data, affirm that LRRC8A contributes to GBM proliferation through its role in Cl^- channel function rather than as a signaling scaffold protein. Yet, interpretations of the effects of VRAC blockers have been called into question due to the limited specificity and/or toxicity of these compounds.[107] Complementary evidence for the importance of $[Cl^-]_i$ in cell proliferation can be found in the anti-proliferative effects of low-Cl^- media.[48,108,109] In the context of GBM, our functional assays showed that LRRC8A knockdown not only potently suppressed VRAC activity but also reduced $[Cl^-]_i$. A similar effect of LRRC8A downregulation on $[Cl^-]_i$ and proliferation was observed in gastric cancer cells.[48] These findings may have mechanistical relevance because recent studies discovered molecular machinery enabling $[Cl^-]_i$-dependent modulation of cellular functions, principally through the atypical kinases from the With-No-lysine(K) family (WNK1-4).[110,111] In WNK isozymes, particularly WNK1 and WNK4, Cl^- binds to the autoinhibitory C-terminal domain and prevents enzymatic activity.[112,113] Consequently, when $[Cl^-]_i$ is reduced, WNKs undergo autophosphorylation and become active. Importantly, WNK1 has emerged as a prominent player in progression of several cancers and is thought to contribute to numerous aspects of tumorigenesis.[87,88,111] Based on the reduction of $[Cl^-]_i$ in LRRC8A knockdown cells, we expected that WNK activity would be increased. Yet, we found no evidence indicating any such effect in our phosphoproteomics assays. Furthermore, the potent WNK inhibitor WNK463 had no influence on cell proliferation despite complete inhibition of WNK activity.

Besides its well-known protein kinase actions, WNK1 may modulate intracellular signaling via a non-enzymatic mechanism (e.g.,[91,92]). Therefore, we additionally tested for the effects of WNK1 siRNA. In striking contrast to the lack of effect of pharmacological inhibitor, WNK1 siRNA knockdown strongly suppressed GBM proliferation. The potential underlying process has been identified only recently. Saha et al.[92] found that the Cl^--bound WNK1 activates mTORC2 through a previously unknown scaffolding mechanism leading to activation of downstream AGC protein kinases, such as SGK1, AKT, and conventional isoforms of PKC.[114] We hypothesize that, in GBM cells, LRRC8A-containing VRAC sustains elevated $[Cl^-]_i$ and facilitates the Cl^--dependent WNK1/mTORC2 scaffolding and downstream signaling. We probed and validated this mechanism using the mTORC1/2 inhibitor KU-0063794 and, alternatively, by blocking the mTORC2-dependent AKT and SGK. Inhibition of mTOR activity, or combinatorial inhibition of

bioRxiv preprint doi: https://doi.org/10.1101/2025.02.02.636139; this version posted February 6, 2025. The copyright holder for this preprint (which was not certified by peer review) is the author/funder, who has granted bioRxiv a license to display the preprint in perpetuity. It is made available under aCC-BY-NC-ND 4.0 International license.

AKT and SGK, fully recapitulated the effect of LRRC8A knockdown, thus firmly supporting the new signaling mechanism presented in Figure 8.

Limitations of the study

In this study, we identified and tested a novel mechanism linking the LRRC8A-containing anion channel VRAC to WNK1/mTORC2-dependent GBM proliferation. There are some limitations of this work, which may be further addressed in future studies. (i) It will be important to probe if the proposed signaling pathway modulates cell growth in a universal or tissue/cell type specific fashion. At this stage there are two additional precedents for the WNK1/mTORC2-dependent regulation of cellular functions in renal tubule cells[92] and myofibroblasts[81]. (ii) It would be helpful to confirm the selective involvement of mTORC2 in the LRRC8A-dependent GBM proliferation using tools of molecular biology (e.g., RNAi) and and perform rescue experiments verifying that LRRC8A, WNK1, and mTORC2 act via a shared mechanism. (iii) One may want to additionally probe for physical interactions between WNK1 and mTORC2 in GBM (such interaction has been firmly established in renal tubule cells[92]). (iv) The transcriptional elements involved in the LRRC8A/WNK1/mTORC2-dependent regulation of GBM proliferation would have to be further explored. (v) The present findings will have to be recapitulated in animal cancer models, which better reflect the complex tumor microenvironment. Finally, (vi) our findings have been thoroughly tested in two patient-derived GBM cell lines only. Although diverse, these cell lines are unlikely to reflect the entire spectrum of GBM heterogeneity. While these caveats can be addressed in future work, they do not alter the major conclusions of the present manuscript.

bioRxiv preprint doi: https://doi.org/10.1101/2025.02.02.636139; this version posted February 6, 2025. The copyright holder for this preprint (which was not certified by peer review) is the author/funder, who has granted bioRxiv a license to display the preprint in perpetuity. It is made available under aCC-BY-NC-ND 4.0 International license.

DECLARATION OF GENERATIVE AI AND AI-ASSISTED TECHNOLOGIES IN WRITING PROCESS

Authors declare that no generative AI or AI-assisted technologies were used in preparing this manuscript. Authors take full responsibility for the content of this publication.

STAR★METHODS

Detailed methods are provided in the online version of this paper and include the following:

- KEY RESOURCES TABLE
- RESOURCES AVAILABILITY
  - Lead contact
  - Materials and availability statement
  - Data and code availability
- EXPERIMENTAL MODEL AND STUDY PARTICIPANTS DETAILS
  - Patient samples
  - Primary GBM cell lines
  - The Cancer Genome Atlas (TCGA) datasets
- METHOD DETAILS
  - Computational analysis of TCGA dataset
  - mRNA isolation and real-time quantitative PCR
  - Protein isolation and Western blot analysis
  - siRNA manipulation of gene expression
  - Radioisotope assay of VRAC activity
  - Cell proliferation assays
  - Measurements of intracellular Cl^- levels
  - Fluorescence-activated cell sorting (FACS) analysis
- QUANTIFICATION AND STATISTICAL ANALYSIS
  - Statistical analyses

SUPPLEMENTAL INFORMATION

The primary data analyzed in this study have been deposited in Open Science Framework and can be found online at https://osf.io/2r7k9

ACKNOWLEDGEMENTS

We are grateful to Drs. David Jourd'heuil, Corinne S. Wilson, and Ryan Kanai for their help with pilot experiments leading to this work. This study was supported in part by the Dr. Louis Sklarow

bioRxiv preprint doi: https://doi.org/10.1101/2025.02.02.636139; this version posted February 6, 2025. The copyright holder for this preprint (which was not certified by peer review) is the author/funder, who has granted bioRxiv a license to display the preprint in perpetuity. It is made available under aCC-BY-NC-ND 4.0 International license.

Memorial Trust, the U.S. National Institutes of Health (grants R01 NS111943 to A.A.M. and R01 HL149993 to N.O.D.), and a translational grant awarded by Albany Medical College (to Y.H.K and A.A.M.).

AUTHOR CONTRIBUTIONS

A.A.M., A.M.F., and M.D.B. conceptualized this study. A.M.F., M.D.B., S.O., N.M., M.A.B., and A.A.M. conducted all included experiments. A.M.F., M.D.B., S.O., I.F.A., A.R.P., Y.H.K., and A.A.M. procured and generated GBM specimens and GBM cell lines. A.M.F., M.D.B., S.O., N.M., A.P.A., M.A.B., N.O.D. and A.A.M. performed data analysis and interpretation. A.A.M., N.O.D., and Y.H.K. acquired funds to support this study. A.A.M. and A.M.F. prepared the initial draft of the manuscript. All authors contributed to manuscript writing and revisions.

DECLARATION OF INTERESTS

The authors report no competing interests.

bioRxiv preprint doi: https://doi.org/10.1101/2025.02.02.636139; this version posted February 6, 2025. The copyright holder for this preprint (which was not certified by peer review) is the author/funder, who has granted bioRxiv a license to display the preprint in perpetuity. It is made available under aCC-BY-NC-ND 4.0 International license.

References

1. Wen, P.Y. and Kesari, S. (2008). Malignant gliomas in adults. N. Engl. J. Med. *359*, 492-507.

2. Brennan, C.W., Verhaak, R.G., McKenna, A., Campos, B., Noushmehr, H., Salama, S.R., Zheng, S., Chakravarty, D., Sanborn, J.Z., Berman, S.H., Beroukhim, R., Bernard, B., Wu, C.J., Genovese, G., Shmulevich, I., Barnholtz-Sloan, J., Zou, L., Vegesna, R., Shukla, S.A., Ciriello, G., Yung, W.K., Zhang, W., Sougnez, C., Mikkelsen, T., Aldape, K., Bigner, D.D., van Meir, E.G., Prados, M., Sloan, A., Black, K.L., Eschbacher, J., Finocchiaro, G., Friedman, W., Andrews, D.W., Guha, A., Iacocca, M., O'Neill, B.P., Foltz, G., Myers, J., Weisenberger, D.J., Penny, R., Kucherlapati, R., Perou, C.M., Hayes, D.N., Gibbs, R., Marra, M., Mills, G.B., Lander, E., Spellman, P., Wilson, R., Sander, C., Weinstein, J., Meyerson, M., Gabriel, S., Laird, P.W., Haussler, D., Getz, G., and Chin, L. (2013). The somatic genomic landscape of glioblastoma. Cell *155*, 462-477.

3. Cloughesy, T.F., Cavenee, W.K., and Mischel, P.S. (2014). Glioblastoma: from molecular pathology to targeted treatment. Annu. Rev. Pathol. *9*, 1-25.

4. Ostrom, Q.T., Price, M., Neff, C., Cioffi, G., Waite, K.A., Kruchko, C., and Barnholtz-Sloan, J.S. (2023). CBTRUS Statistical Report: Primary Brain and Other Central Nervous System Tumors Diagnosed in the United States in 2016-2020. Neuro. Oncol. *25*, iv1-iv99.

5. Tan, A.C., Ashley, D.M., Lopez, G.Y., Malinzak, M., Friedman, H.S., and Khasraw, M. (2020). Management of glioblastoma: State of the art and future directions. CA Cancer J. Clin. *70*, 299-312.

6. Stupp, R., Mason, W.P., van den Bent, M.J., Weller, M., Fisher, B., Taphoorn, M.J., Belanger, K., Brandes, A.A., Marosi, C., Bogdahn, U., Curschmann, J., Janzer, R.C., Ludwin, S.K., Gorlia, T., Allgeier, A., Lacombe, D., Cairncross, J.G., Eisenhauer, E., and Mirimanoff, R.O. (2005). Radiotherapy plus concomitant and adjuvant temozolomide for glioblastoma. N. Engl. J. Med. *352*, 987-996.

7. Omuro, A. and DeAngelis, L.M. (2013). Glioblastoma and other malignant gliomas: a clinical review. JAMA *310*, 1842-1850.

8. Alexander, B.M. and Cloughesy, T.F. (2017). Adult Glioblastoma. J. Clin. Oncol. *35*, 2402-2409.

9. Stupp, R., Taillibert, S., Kanner, A., Read, W., Steinberg, D., Lhermitte, B., Toms, S., Idbaih, A., Ahluwalia, M.S., Fink, K., Di, M.F., Lieberman, F., Zhu, J.J., Stragliotto, G., Tran, D., Brem, S., Hottinger, A., Kirson, E.D., Lavy-Shahaf, G., Weinberg, U., Kim, C.Y., Paek, S.H., Nicholas, G., Bruna, J., Hirte, H., Weller, M., Palti, Y., Hegi, M.E., and Ram, Z. (2017). Effect of Tumor-Treating Fields Plus Maintenance Temozolomide vs Maintenance Temozolomide Alone on Survival in Patients With Glioblastoma: A Randomized Clinical Trial. JAMA *318*, 2306-2316.

bioRxiv preprint doi: https://doi.org/10.1101/2025.02.02.636139; this version posted February 6, 2025. The copyright holder for this preprint (which was not certified by peer review) is the author/funder, who has granted bioRxiv a license to display the preprint in perpetuity. It is made available under aCC-BY-NC-ND 4.0 International license.

10. Desjardins, A., Gromeier, M., Herndon, J.E., Beaubier, N., Bolognesi, D.P., Friedman, A.H., Friedman, H.S., McSherry, F., Muscat, A.M., Nair, S., Peters, K.B., Randazzo, D., Sampson, J.H., Vlahovic, G., Harrison, W.T., McLendon, R.E., Ashley, D., and Bigner, D.D. (2018). Recurrent Glioblastoma Treated with Recombinant Poliovirus. N. Engl. J. Med. *379*, 150-161.

11. Liau, L.M., Ashkan, K., Brem, S., Campian, J.L., Trusheim, J.E., Iwamoto, F.M., Tran, D.D., Ansstas, G., Cobbs, C.S., Heth, J.A., Salacz, M.E., D'Andre, S., Aiken, R.D., Moshel, Y.A., Nam, J.Y., Pillainayagam, C.P., Wagner, S.A., Walter, K.A., Chaudhary, R., Goldlust, S.A., Lee, I.Y., Bota, D.A., Elinzano, H., Grewal, J., Lillehei, K., Mikkelsen, T., Walbert, T., Abram, S., Brenner, A.J., Ewend, M.G., Khagi, S., Lovick, D.S., Portnow, J., Kim, L., Loudon, W.G., Martinez, N.L., Thompson, R.C., Avigan, D.E., Fink, K.L., Geoffroy, F.J., Giglio, P., Gligich, O., Krex, D., Lindhorst, S.M., Lutzky, J., Meisel, H.J., Nadji-Ohl, M., Sanchin, L., Sloan, A., Taylor, L.P., Wu, J.K., Dunbar, E.M., Etame, A.B., Kesari, S., Mathieu, D., Piccioni, D.E., Baskin, D.S., Lacroix, M., May, S.A., New, P.Z., Pluard, T.J., Toms, S.A., Tse, V., Peak, S., Villano, J.L., Battiste, J.D., Mulholland, P.J., Pearlman, M.L., Petrecca, K., Schulder, M., Prins, R.M., Boynton, A.L., and Bosch, M.L. (2023). Association of Autologous Tumor Lysate-Loaded Dendritic Cell Vaccination With Extension of Survival Among Patients With Newly Diagnosed and Recurrent Glioblastoma: A Phase 3 Prospective Externally Controlled Cohort Trial. JAMA Oncol. *9*, 112-121.

12. Lim, M., Xia, Y., Bettegowda, C., and Weller, M. (2018). Current state of immunotherapy for glioblastoma. Nat. Rev. Clin. Oncol. *15*, 422-442.

13. Wen, P.Y., Touat, M., Alexander, B.M., Mellinghoff, I.K., Ramkissoon, S., McCluskey, C.S., Pelton, K., Haidar, S., Basu, S.S., Gaffey, S.C., Brown, L.E., Martinez-Ledesma, J.E., Wu, S., Kim, J., Wei, W., Park, M.A., Huse, J.T., Kuhn, J.G., Rinne, M.L., Colman, H., Agar, N.Y.R., Omuro, A.M., DeAngelis, L.M., Gilbert, M.R., de Groot, J.F., Cloughesy, T.F., Chi, A.S., Roberts, T.M., Zhao, J.J., Lee, E.Q., Nayak, L., Heath, J.R., Horky, L.L., Batchelor, T.T., Beroukhim, R., Chang, S.M., Ligon, A.H., Dunn, I.F., Koul, D., Young, G.S., Prados, M.D., Reardon, D.A., Yung, W.K.A., and Ligon, K.L. (2019). Buparlisib in Patients With Recurrent Glioblastoma Harboring Phosphatidylinositol 3-Kinase Pathway Activation: An Open-Label, Multicenter, Multi-Arm, Phase II Trial. J. Clin. Oncol. *37*, 741-750.

14. Pridham, K.J., Hutchings, K.R., Beck, P., Liu, M., Xu, E., Saechin, E., Bui, V., Patel, C., Solis, J., Huang, L., Tegge, A., Kelly, D.F., and Sheng, Z. (2024). Selective regulation of chemosensitivity in glioblastoma by phosphatidylinositol 3-kinase beta. iScience. *27*, 109921-

15. Litan, A. and Langhans, S.A. (2015). Cancer as a channelopathy: ion channels and pumps in tumor development and progression. Front Cell Neurosci. *9*, 86-

16. Prevarskaya, N., Skryma, R., and Shuba, Y. (2018). Ion channels in cancer: are cancer hallmarks oncochannelopathies? Physiol Rev. *98*, 559-621.

17. Harraz, O.F. and Delpire, E. (2024). Recent insights into channelopathies. Physiol Rev. *104*, 23-31.

18. Kunzelmann, K. (2005). Ion channels and cancer. J. Membr. Biol. *205*, 159-173.

bioRxiv preprint doi: https://doi.org/10.1101/2025.02.02.636139; this version posted February 6, 2025. The copyright holder for this preprint (which was not certified by peer review) is the author/funder, who has granted bioRxiv a license to display the preprint in perpetuity. It is made available under aCC-BY-NC-ND 4.0 International license.

19. Becchetti, A. (2011). Ion channels and transporters in cancer. 1. Ion channels and cell proliferation in cancer. Am. J. Physiol Cell Physiol *301*, C255-C265.

20. Cuddapah, V.A. and Sontheimer, H. (2011). Ion channels and tranporters in cancer. 2. Ion channels and the control of cancer cell migration. Am. J. Physiol Cell Physiol *301*, C541-C549.

21. Bortner, C.D. and Cidlowski, J.A. (2014). Ion channels and apoptosis in cancer. Philos. Trans. R. Soc. Lond B Biol. Sci. *369*, 20130104-

22. Hoffmann, E.K. and Lambert, I.H. (2014). Ion channels and transporters in the development of drug resistance in cancer cells. Philos. Trans. R. Soc. Lond. B Biol. Sci. *369*, 20130109-

23. Sontheimer, H. (2008). An unexpected role for ion channels in brain tumor metastasis. Exp. Biol. Med. (Maywood.) *233*, 779-791.

24. Duran, C., Thompson, C.H., Xiao, Q., and Hartzell, H.C. (2010). Chloride channels: often enigmatic, rarely predictable. Annu. Rev. Physiol *72*, 95-121.

25. Turner, K.L. and Sontheimer, H. (2014). Cl- and K+ channels and their role in primary brain tumour biology. Philos. Trans. R. Soc. Lond B Biol. Sci. *369*, 20130095-

26. Nilius, B., Eggermont, J., Voets, T., Buyse, G., Manolopoulos, V., and Droogmans, G. (1997). Properties of volume-regulated anion channels in mammalian cells. Prog. Biophys. Mol. Biol. *68*, 69-119.

27. Pedersen, S.F., Okada, Y., and Nilius, B. (2016). Biophysics and physiology of the volume-regulated anion channel (VRAC)/volume-sensitive outwardly rectifying anion channel (VSOR). Pflugers Arch. *468*, 371-383.

28. Ullrich, N. and Sontheimer, H. (1996). Biophysical and pharmacological characterization of chloride currents in human astrocytoma cells. Am. J. Physiol *270*, C1511-C1521.

29. McFerrin, M.B. and Sontheimer, H. (2006). A role for ion channels in glioma cell invasion. Neuron Glia Biol. *2*, 39-49.

30. Caramia, M., Sforna, L., Franciolini, F., and Catacuzzeno, L. (2019). The volume-regulated anion channel in glioblastoma. Cancers. (Basel) *11*,

31. Strange, K., Emma, F., and Jackson, P.S. (1996). Cellular and molecular physiology of volume-sensitive anion channels. Am. J. Physiol *270*, C711-C730.

32. Okada, Y. (1997). Volume expansion-sensing outward-rectifier Cl- channel: fresh start to the molecular identity and volume sensor. Am. J. Physiol. Cell Physiol. *273*, C755-C789.

33. Shen, M.R., Droogmans, G., Eggermont, J., Voets, T., Ellory, J.C., and Nilius, B. (2000). Differential expression of volume-regulated anion channels during cell cycle progression of human cervical cancer cells. J. Physiol. *529*, 385-394.

bioRxiv preprint doi: https://doi.org/10.1101/2025.02.02.636139; this version posted February 6, 2025. The copyright holder for this preprint (which was not certified by peer review) is the author/funder, who has granted bioRxiv a license to display the preprint in perpetuity. It is made available under aCC-BY-NC-ND 4.0 International license.

34. Maeno, E., Ishizaki, Y., Kanaseki, T., Hazama, A., and Okada, Y. (2000). Normotonic cell shrinkage because of disordered volume regulation is an early prerequisite to apoptosis. Proc. Natl. Acad. Sci. U. S. A. *97*, 9487-9492.

35. Okada, Y., Maeno, E., Shimizu, T., Dezaki, K., Wang, J., and Morishima, S. (2001). Receptor-mediated control of regulatory volume decrease (RVD) and apoptotic volume decrease (AVD). J. Physiol. *532*, 3-16.

36. Pedersen, S.F., Klausen, T.K., and Nilius, B. (2015). The identification of a volume-regulated anion channel: an amazing Odyssey. Acta Physiol (Oxf) *213*, 868-881.

37. Qiu, Z., Dubin, A.E., Mathur, J., Tu, B., Reddy, K., Miraglia, L.J., Reinhardt, J., Orth, A.P., and Patapoutian, A. (2014). SWELL1, a plasma membrane protein, is an essential component of volume-regulated anion channel. Cell *157*, 447-458.

38. Voss, F.K., Ullrich, F., Munch, J., Lazarow, K., Lutter, D., Mah, N., Andrade-Navarro, M.A., von Kries, J.P., Stauber, T., and Jentsch, T.J. (2014). Identification of LRRC8 heteromers as an essential component of the volume-regulated anion channel VRAC. Science *344*, 634-638.

39. Kumar, L., Chou, J., Yee, C.S., Borzutzky, A., Vollmann, E.H., von Andrian, U.H., Park, S.Y., Hollander, G., Manis, J.P., Poliani, P.L., and Geha, R.S. (2014). Leucine-rich repeat containing 8A (LRRC8A) is essential for T lymphocyte development and function. J. Exp. Med. *211*, 929-942.

40. Zhang, Y., Xie, L., Gunasekar, S.K., Tong, D., Mishra, A., Gibson, W.J., Wang, C., Fidler, T., Marthaler, B., Klingelhutz, A., Abel, E.D., Samuel, I., Smith, J.K., Cao, L., and Sah, R. (2017). SWELL1 is a regulator of adipocyte size, insulin signalling and glucose homeostasis. Nat. Cell Biol. *19*, 504-517.

41. Kumar, A., Xie, L., Ta, C.M., Hinton, A.O., Gunasekar, S.K., Minerath, R.A., Shen, K., Maurer, J.M., Grueter, C.E., Abel, E.D., Meyer, G., and Sah, R. (2020). SWELL1 regulates skeletal muscle cell size, intracellular signaling, adiposity and glucose metabolism. eLife *9*,

42. Alghanem, A.F., Abello, J., Maurer, J.M., Kumar, A., Ta, C.M., Gunasekar, S.K., Fatima, U., Kang, C., Xie, L., Adeola, O., Riker, M., Elliot-Hudson, M., Minerath, R.A., Grueter, C.E., Mullins, R.F., Stratman, A.N., and Sah, R. (2021). The SWELL1-LRRC8 complex regulates endothelial AKT-eNOS signaling and vascular function. eLife *10*, e61313-

43. Bao, J., Perez, C.J., Kim, J., Zhang, H., Murphy, C.J., Hamidi, T., Jaubert, J., Platt, C.D., Chou, J., Deng, M., Zhou, M.H., Huang, Y., Gaitan-Penas, H., Guenet, J.L., Lin, K., Lu, Y., Chen, T., Bedford, M.T., Dent, S.Y., Richburg, J.H., Estevez, R., Pan, H.L., Geha, R.S., Shi, Q., and Benavides, F. (2018). Deficient LRRC8A-dependent volume-regulated anion channel activity is associated with male infertility in mice. JCI. Insight. *3*,

44. Yang, J., Vitery, M.D.C., Chen, J., Osei-Owusu, J., Chu, J., and Qiu, Z. (2019). Glutamate-Releasing SWELL1 Channel in Astrocytes Modulates Synaptic Transmission and Promotes Brain Damage in Stroke. Neuron *102*, 813-827.

bioRxiv preprint doi: https://doi.org/10.1101/2025.02.02.636139; this version posted February 6, 2025. The copyright holder for this preprint (which was not certified by peer review) is the author/funder, who has granted bioRxiv a license to display the preprint in perpetuity. It is made available under aCC-BY-NC-ND 4.0 International license.

45. Zhou, C., Chen, X., Planells-Cases, R., Chu, J., Wang, L., Cao, L., Li, Z., Lopez-Cayuqueo, K.I., Xie, Y., Ye, S., Wang, X., Ullrich, F., Ma, S., Fang, Y., Zhang, X., Qian, Z., Liang, X., Cai, S.Q., Jiang, Z., Zhou, D., Leng, Q., Xiao, T.S., Lan, K., Yang, J., Li, H., Peng, C., Qiu, Z., Jentsch, T.J., and Xiao, H. (2020). Transfer of cGAMP into bystander cells via LRRC8 volume-regulated anion channels augments STING-mediated interferon responses and anti-viral immunity. Immunity *52*, 767-781.

46. Konishi, T., Shiozaki, A., Kosuga, T., Kudou, M., Shoda, K., Arita, T., Konishi, H., Komatsu, S., Kubota, T., Fujiwara, H., Okamoto, K., Kishimoto, M., Konishi, E., Marunaka, Y., and Otsuji, E. (2019). LRRC8A expression influences growth of esophageal squamous cell carcinoma. Am. J. Pathol. *189*, 1973-1985.

47. Lu, P., Ding, Q., Li, X., Ji, X., Li, L., Fan, Y., Xia, Y., Tian, D., and Liu, M. (2019). SWELL1 promotes cell growth and metastasis of hepatocellular carcinoma in vitro and in vivo. EBioMedicine. *48*, 100-116.

48. Kurashima, K., Shiozaki, A., Kudou, M., Shimizu, H., Arita, T., Kosuga, T., Konishi, H., Komatsu, S., Kubota, T., Fujiwara, H., Okamoto, K., Kishimoto, M., Konishi, E., and Otsuji, E. (2021). LRRC8A influences the growth of gastric cancer cells via the p53 signaling pathway. Gastric. Cancer *24*, 1063-1075.

49. Chen, Y., Zuo, X., Wei, Q., Xu, J., Liu, X., Liu, S., Wang, H., Luo, Q., Wang, Y., Yang, Y., Zhao, H., Xu, J., Liu, T., and Yi, P. (2023). Upregulation of LRRC8A by m(5)C modification-mediated mRNA stability suppresses apoptosis and facilitates tumorigenesis in cervical cancer. Int. J. Biol. Sci. *19*, 691-704.

50. Rubino, S., Bach, M.D., Schober, A.L., Lambert, I.H., and Mongin, A.A. (2018). Downregulation of Leucine-Rich Repeat-Containing 8A limits proliferation and increases sensitivity of glioblastoma to temozolomide and carmustine. Front. Oncol. *8*, 142-

51. Zhang, Y., Sloan, S.A., Clarke, L.E., Caneda, C., Plaza, C.A., Blumenthal, P.D., Vogel, H., Steinberg, G.K., Edwards, M.S., Li, G., Duncan, J.A., III, Cheshier, S.H., Shuer, L.M., Chang, E.F., Grant, G.A., Gephart, M.G., and Barres, B.A. (2016). Purification and characterization of progenitor and mature human astrocytes reveals transcriptional and functional differences with mouse. Neuron *89*, 37-53.

52. Ohgaki, H. and Kleihues, P. (2013). The definition of primary and secondary glioblastoma. Clin. Cancer Res. *19*, 764-772.

53. Latowska-Lysiak, J., Zarebska, Z., Sajek, M.P., Grabowska, A., Buratin, A., Misiorek, J.O., Kuczynski, K., Bortoluzzi, S., Zywicki, M., Kosinski, J.G., Rybak-Wolf, A., Piestrzeniewicz, R., Barciszewska, A.M., and Rolle, K. (2024). Transcriptome-wide analysis of circRNA and RBP profiles and their molecular and clinical relevance for GBM. bioRxiv *doi: 10.1101/2024.06.12.598692*,

54. Kimelberg, H.K., Rutledge, E., Goderie, S., and Charniga, C. (1995). Astrocytic swelling due to hypotonic or high K+ medium causes inhibition of glutamate and aspartate uptake and increases their release. J. Cereb. Blood Flow Metab *15*, 409-416. Anion channel; Volume regulation.

bioRxiv preprint doi: https://doi.org/10.1101/2025.02.02.636139; this version posted February 6, 2025. The copyright holder for this preprint (which was not certified by peer review) is the author/funder, who has granted bioRxiv a license to display the preprint in perpetuity. It is made available under aCC-BY-NC-ND 4.0 International license.

55. Abdullaev, I.F., Rudkouskaya, A., Schools, G.P., Kimelberg, H.K., and Mongin, A.A. (2006). Pharmacological comparison of swelling-activated excitatory amino acid release and Cl- currents in rat cultured astrocytes. J. Physiol. *572*, 677-689.

56. Hyzinski-Garcia, M.C., Rudkouskaya, A., and Mongin, A.A. (2014). LRRC8A protein is indispensable for swelling-activated and ATP-induced release of excitatory amino acids in rat astrocytes. J. Physiol. *592*, 4855-4862.

57. Wilson, C.S., Dohare, P., Orbeta, S., Nalwalk, J.W., Huang, Y., Ferland, R.J., Sah, R., Scimemi, A., and Mongin, A.A. (2021). Late adolescence mortality in mice with brain-specific deletion of the volume-regulated anion channel subunit LRRC8A. FASEB J. *35*, e21869-

58. Love, M.I., Huber, W., and Anders, S. (2014). Moderated estimation of fold change and dispersion for RNA-seq data with DESeq2. Genome Biol. *15*, 550-

59. Dillies, M.A., Rau, A., Aubert, J., Hennequet-Antier, C., Jeanmougin, M., Servant, N., Keime, C., Marot, G., Castel, D., Estelle, J., Guernec, G., Jagla, B., Jouneau, L., Laloe, D., Le, G.C., Schaeffer, B., Le, C.S., Guedj, M., and Jaffrezic, F. (2013). A comprehensive evaluation of normalization methods for Illumina high-throughput RNA sequencing data analysis. Brief. Bioinform. *14*, 671-683.

60. Zhao, Y., Li, M.C., Konate, M.M., Chen, L., Das, B., Karlovich, C., Williams, P.M., Evrard, Y.A., Doroshow, J.H., and McShane, L.M. (2021). TPM, FPKM, or Normalized Counts? A Comparative Study of Quantification Measures for the Analysis of RNA-seq Data from the NCI Patient-Derived Models Repository. J. Transl. Med. *19*, 269-

61. Chen, X., Zhang, F., Hu, G., Li, X., Wang, L., Li, C., Huo, C., Xu, R., Hou, L., Wang, N., and Wang, X. (2022). LRRC8A critically regulates myofibroblast phenotypes and fibrotic remodeling following myocardial infarction. Theranostics. *12*, 5824-5835.

62. Karin, M. (1995). The regulation of AP-1 activity by mitogen-activated protein kinases. J. Biol. Chem. *270*, 16483-16486.

63. Buday, L. and Downward, J. (1993). Epidermal growth factor regulates p21ras through the formation of a complex of receptor, Grb2 adapter protein, and Sos nucleotide exchange factor. Cell *73*, 611-620.

64. Scita, G., Tenca, P., Frittoli, E., Tocchetti, A., Innocenti, M., Giardina, G., and Di Fiore, P.P. (2000). Signaling from Ras to Rac and beyond: not just a matter of GEFs. EMBO J. *19*, 2393-2398.

65. Innocenti, M., Tenca, P., Frittoli, E., Faretta, M., Tocchetti, A., Di Fiore, P.P., and Scita, G. (2002). Mechanisms through which Sos-1 coordinates the activation of Ras and Rac. J. Cell Biol. *156*, 125-136.

66. Adams, S.J., Aydin, I.T., and Celebi, J.T. (2012). GAB2--a scaffolding protein in cancer. Mol. Cancer Res. *10*, 1265-1270.

67. Martini, M., De Santis, M.C., Braccini, L., Gulluni, F., and Hirsch, E. (2014). PI3K/AKT signaling pathway and cancer: an updated review. Ann. Med. *46*, 372-383.

bioRxiv preprint doi: https://doi.org/10.1101/2025.02.02.636139; this version posted February 6, 2025. The copyright holder for this preprint (which was not certified by peer review) is the author/funder, who has granted bioRxiv a license to display the preprint in perpetuity. It is made available under aCC-BY-NC-ND 4.0 International license.

68. Davies, S.P., Reddy, H., Caivano, M., and Cohen, P. (2000). Specificity and mechanism of action of some commonly used protein kinase inhibitors. Biochem. J. *351*, 95-105.

69. Gilmartin, A.G., Bleam, M.R., Groy, A., Moss, K.G., Minthorn, E.A., Kulkarni, S.G., Rominger, C.M., Erskine, S., Fisher, K.E., Yang, J., Zappacosta, F., Annan, R., Sutton, D., and Laquerre, S.G. (2011). GSK1120212 (JTP-74057) is an inhibitor of MEK activity and activation with favorable pharmacokinetic properties for sustained in vivo pathway inhibition. Clin. Cancer Res. *17*, 989-1000.

70. Bennett, B.L., Sasaki, D.T., Murray, B.W., O'Leary, E.C., Sakata, S.T., Xu, W., Leisten, J.C., Motiwala, A., Pierce, S., Satoh, Y., Bhagwat, S.S., Manning, A.M., and Anderson, D.W. (2001). SP600125, an anthrapyrazolone inhibitor of Jun N-terminal kinase. Proc. Natl. Acad. Sci. U. S. A *98*, 13681-13686.

71. Jiang, J., Jiang, B., He, Z., Ficarro, S.B., Che, J., Marto, J.A., Gao, Y., Zhang, T., and Gray, N.S. (2020). Discovery of covalent MKK4/7 dual inhibitor. Cell Chem. Biol. *27*, 1553-1560.

72. Potapova, O., Gorospe, M., Bost, F., Dean, N.M., Gaarde, W.A., Mercola, D., and Holbrook, N.J. (2000). c-Jun N-terminal kinase is essential for growth of human T98G glioblastoma cells. J. Biol. Chem. *275*, 24767-24775.

73. Matsuda, K., Sato, A., Okada, M., Shibuya, K., Seino, S., Suzuki, K., Watanabe, E., Narita, Y., Shibui, S., Kayama, T., and Kitanaka, C. (2012). Targeting JNK for therapeutic depletion of stem-like glioblastoma cells. Sci. Rep. *2*, 516-

74. Ruvinsky, I. and Meyuhas, O. (2006). Ribosomal protein S6 phosphorylation: from protein synthesis to cell size. Trends Biochem. Sci. *31*, 342-348.

75. Sehgal, S.N. (2003). Sirolimus: its discovery, biological properties, and mechanism of action. Transplant. Proc. *35*, 7S-14S.

76. Garcia-Martinez, J.M., Moran, J., Clarke, R.G., Gray, A., Cosulich, S.C., Chresta, C.M., and Alessi, D.R. (2009). Ku-0063794 is a specific inhibitor of the mammalian target of rapamycin (mTOR). Biochem. J. *421*, 29-42.

77. Gharbi, S.I., Zvelebil, M.J., Shuttleworth, S.J., Hancox, T., Saghir, N., Timms, J.F., and Waterfield, M.D. (2007). Exploring the specificity of the PI3K family inhibitor LY294002. Biochem. J. *404*, 15-21.

78. Habela, C.W., Ernest, N.J., Swindall, A.F., and Sontheimer, H. (2009). Chloride accumulation drives volume dynamics underlying cell proliferation and migration. J. Neurophysiol. *101*, 750-757.

79. Li, Y., Sanchez Trivino, C.A., Hernandez, A., Mortal, S., Spada, F., Krivosheia, I., Franco, N., Spelat, R., Cesselli, D., Manini, I., Skrap, M., Menini, A., Cesca, F., and Torre, V. (2024). Mechanisms of Glioblastoma Replication: Ca2+ Flares and Cl- Currents. Mol. Cancer Res. *22*, 852-863.

bioRxiv preprint doi: https://doi.org/10.1101/2025.02.02.636139; this version posted February 6, 2025. The copyright holder for this preprint (which was not certified by peer review) is the author/funder, who has granted bioRxiv a license to display the preprint in perpetuity. It is made available under aCC-BY-NC-ND 4.0 International license.

80. Su, G., Kintner, D.B., and Sun, D. (2002). Contribution of Na(+)-K(+)-Cl(-) cotransporter to high-[K(+)](o)- induced swelling and EAA release in astrocytes. Am. J. Physiol Cell Physiol *282*, C1136-C1146.

81. Reed, E.B., Orbeta, S., Miao, B.A., Sitikov, A., Chen, B., Levitan, I., Solway, J., Mutlu, G.M., Fang, Y., Mongin, A.A., and Dulin, N.O. (2024). Anoctamin-1 is induced by TGF-beta and contributes to lung myofibroblast differentiation. Am. J. Physiol Lung Cell Mol. Physiol *326*, L111-L123.

82. Dick, G.M., Kong, I.D., and Sanders, K.M. (1999). Effects of anion channel antagonists in canine colonic myocytes: comparative pharmacology of Cl-, Ca2+ and K+ currents. Br. J. Pharmacol. *127*, 1819-1831.

83. Helix, N., Strobaek, D., Dahl, B.H., and Christophersen, P. (2003). Inhibition of the endogenous volume-regulated anion channel (VRAC) in HEK293 cells by acidic di-aryl-ureas. J. Membr. Biol. *196*, 83-94.

84. Afzal, A., Figueroa, E.E., Kharade, S.V., Bittman, K., Matlock, B.K., Flaherty, D.K., and Denton, J.S. (2019). The LRRC8 volume-regulated anion channel inhibitor, DCPIB, inhibits mitochondrial respiration independently of the channel. Physiol Rep. *7*, e14303-

85. Gagnon, K.B. and Delpire, E. (2012). Molecular physiology of SPAK and OSR1: two Ste20-related protein kinases regulating ion transport. Physiol Rev. *92*, 1577-1617.

86. Zagorska, A., Pozo-Guisado, E., Boudeau, J., Vitari, A.C., Rafiqi, F.H., Thastrup, J., Deak, M., Campbell, D.G., Morrice, N.A., Prescott, A.R., and Alessi, D.R. (2007). Regulation of activity and localization of the WNK1 protein kinase by hyperosmotic stress. J. Cell Biol. *176*, 89-100.

87. Moniz, S. and Jordan, P. (2010). Emerging roles for WNK kinases in cancer. Cell Mol. Life Sci. *67*, 1265-1276.

88. Jung, J.U., Jaykumar, A.B., and Cobb, M.H. (2022). WNK1 in Malignant Behaviors: A Potential Target for Cancer? Front Cell Dev. Biol. *10*, 935318-

89. Yamada, K., Park, H.M., Rigel, D.F., DiPetrillo, K., Whalen, E.J., Anisowicz, A., Beil, M., Berstler, J., Brocklehurst, C.E., Burdick, D.A., Caplan, S.L., Capparelli, M.P., Chen, G., Chen, W., Dale, B., Deng, L., Fu, F., Hamamatsu, N., Harasaki, K., Herr, T., Hoffmann, P., Hu, Q.Y., Huang, W.J., Idamakanti, N., Imase, H., Iwaki, Y., Jain, M., Jeyaseelan, J., Kato, M., Kaushik, V.K., Kohls, D., Kunjathoor, V., LaSala, D., Lee, J., Liu, J., Luo, Y., Ma, F., Mo, R., Mowbray, S., Mogi, M., Ossola, F., Pandey, P., Patel, S.J., Raghavan, S., Salem, B., Shanado, Y.H., Trakshel, G.M., Turner, G., Wakai, H., Wang, C., Weldon, S., Wielicki, J.B., Xie, X., Xu, L., Yagi, Y.I., Yasoshima, K., Yin, J., Yowe, D., Zhang, J.H., Zheng, G., and Monovich, L. (2016). Small-molecule WNK inhibition regulates cardiovascular and renal function. Nat. Chem. Biol. *12*, 896-898.

90. Tu, S.W., Bugde, A., Luby-Phelps, K., and Cobb, M.H. (2011). WNK1 is required for mitosis and abscission. Proc. Natl. Acad. Sci. U. S. A *108*, 1385-1390.

bioRxiv preprint doi: https://doi.org/10.1101/2025.02.02.636139; this version posted February 6, 2025. The copyright holder for this preprint (which was not certified by peer review) is the author/funder, who has granted bioRxiv a license to display the preprint in perpetuity. It is made available under aCC-BY-NC-ND 4.0 International license.

91. Xu, B.E., Stippec, S., Lazrak, A., Huang, C.L., and Cobb, M.H. (2005). WNK1 activates SGK1 by a phosphatidylinositol 3-kinase-dependent and non-catalytic mechanism. J. Biol. Chem. *280*, 34218-34223.

92. Saha, B., Leite-Dellova, D.C.A., Demko, J., Sorensen, M.V., Takagi, E., Gleason, C.E., Shabbir, W., and Pearce, D. (2022). WNK1 is a chloride-stimulated scaffold that regulates mTORC2 activity and ion transport. J. Cell Sci. *135*,

93. Sarbassov, D.D., Guertin, D.A., Ali, S.M., and Sabatini, D.M. (2005). Phosphorylation and regulation of Akt/PKB by the rictor-mTOR complex. Science *307*, 1098-1101.

94. Hirai, H., Sootome, H., Nakatsuru, Y., Miyama, K., Taguchi, S., Tsujioka, K., Ueno, Y., Hatch, H., Majumder, P.K., Pan, B.S., and Kotani, H. (2010). MK-2206, an allosteric Akt inhibitor, enhances antitumor efficacy by standard chemotherapeutic agents or molecular targeted drugs in vitro and in vivo. Mol. Cancer Ther. *9*, 1956-1967.

95. Sherk, A.B., Frigo, D.E., Schnackenberg, C.G., Bray, J.D., Laping, N.J., Trizna, W., Hammond, M., Patterson, J.R., Thompson, S.K., Kazmin, D., Norris, J.D., and McDonnell, D.P. (2008). Development of a small-molecule serum- and glucocorticoid-regulated kinase-1 antagonist and its evaluation as a prostate cancer therapeutic. Cancer Res. *68*, 7475-7483.

96. Lawlor, M.A. and Alessi, D.R. (2001). PKB/Akt: a key mediator of cell proliferation, survival and insulin responses? J. Cell Sci. *114*, 2903-2910.

97. Zhang, H., Deng, Z., Zhang, D., Li, H., Zhang, L., Niu, J., Zuo, W., Fu, R., Fan, L., Ye, J.H., and She, J. (2018). High expression of leucine-rich repeat-containing 8A is indicative of a worse outcome of colon cancer patients by enhancing cancer cell growth and metastasis. Oncol. Rep. *40*, 1275-1286.

98. Xu, R., Hu, Y., Xie, Q., Zhang, C., Zhao, Y., Zhang, H., Shi, H., Wang, X., and Shi, C. (2022). LRRC8A is a promising prognostic biomarker and therapeutic target for pancreatic adenocarcinoma. Cancers. (Basel) *14*,

99. Carpanese, V., Festa, M., Prosdocimi, E., Bachmann, M., Sadeghi, S., Bertelli, S., Stein, F., Velle, A., Abdel-Salam, M.A.L., Romualdi, C., Pusch, M., and Checchetto, V. (2024). Interactomic exploration of LRRC8A in volume-regulated anion channels. Cell Death. Discov. *10*, 299-

100. Liu, T. and Stauber, T. (2019). The volume-regulated anion channel LRRC8/VRAC is dispensable for cell proliferation and migration. Int. J. Mol. Sci. *20*,

101. Lemmon, M.A. and Schlessinger, J. (2010). Cell signaling by receptor tyrosine kinases. Cell *141*, 1117-1134.

102. Giubellino, A., Burke, T.R., Jr., and Bottaro, D.P. (2008). Grb2 signaling in cell motility and cancer. Expert. Opin. Ther. Targets. *12*, 1021-1033.

103. Wondergem, R., Gong, W., Monen, S.H., Dooley, S.N., Gonce, J.L., Conner, T.D., Houser, M., Ecay, T.W., and Ferslew, K.E. (2001). Blocking swelling-activated chloride current inhibits mouse liver cell proliferation. J. Physiol. *532*, 661-672.

bioRxiv preprint doi: https://doi.org/10.1101/2025.02.02.636139; this version posted February 6, 2025. The copyright holder for this preprint (which was not certified by peer review) is the author/funder, who has granted bioRxiv a license to display the preprint in perpetuity. It is made available under aCC-BY-NC-ND 4.0 International license.

104. Wong, R., Chen, W., Zhong, X., Rutka, J.T., Feng, Z.P., and Sun, H.S. (2018). Swelling-induced chloride current in glioblastoma proliferation, migration, and invasion. J. Cell Physiol. *233*, 363-370.

105. Lang, F., Foller, M., Lang, K., Lang, P., Ritter, M., Vereninov, A., Szabo, I., Huber, S.M., and Gulbins, E. (2007). Cell volume regulatory ion channels in cell proliferation and cell death. Methods Enzymol. *428*, 209-225.

106. Chen, L., Becker, T.M., Koch, U., and Stauber, T. (2019). The LRRC8/VRAC anion channel facilitates myogenic differentiation of murine myoblasts by promoting membrane hyperpolarization. J. Biol. Chem.

107. Figueroa, E.E. and Denton, J.S. (2022). A SWELL time to develop the molecular pharmacology of the volume-regulated anion channel (VRAC). Channels (Austin.) *16*, 27-36.

108. Miyazaki, H., Shiozaki, A., Niisato, N., Ohsawa, R., Itoi, H., Ueda, Y., Otsuji, E., Yamagishi, H., Iwasaki, Y., Nakano, T., Nakahari, T., and Marunaka, Y. (2008). Chloride ions control the G1/S cell-cycle checkpoint by regulating the expression of p21 through a p53-independent pathway in human gastric cancer cells. Biochem. Biophys. Res. Commun. *366*, 506-512.

109. Klausen, T.K., Preisler, S., Pedersen, S.F., and Hoffmann, E.K. (2010). Monovalent ions control proliferation of Ehrlich Lettre ascites cells. Am. J. Physiol. Cell Physiol. *299*, C714-C725.

110. McCormick, J.A. and Ellison, D.H. (2011). The WNKs: atypical protein kinases with pleiotropic actions. Physiol Rev. *91*, 177-219.

111. Shekarabi, M., Zhang, J., Khanna, A.R., Ellison, D.H., Delpire, E., and Kahle, K.T. (2017). WNK kinase signaling in ion homeostasis and human disease. Cell Metab *25*, 285-299.

112. Piala, A.T., Moon, T.M., Akella, R., He, H., Cobb, M.H., and Goldsmith, E.J. (2014). Chloride sensing by WNK1 involves inhibition of autophosphorylation. Sci. Signal. *7*, ra41-

113. Terker, A.S., Zhang, C., Erspamer, K.J., Gamba, G., Yang, C.L., and Ellison, D.H. (2016). Unique chloride-sensing properties of WNK4 permit the distal nephron to modulate potassium homeostasis. Kidney Int. *89*, 127-134.

114. Alessi, D.R., Pearce, L.R., and Garcia-Martinez, J.M. (2009). New insights into mTOR signaling: mTORC2 and beyond. Sci. Signal. *2*, e27-

115. (2013). World Medical Association Declaration of Helsinki: ethical principles for medical research involving human subjects. JAMA *310*, 2191-2194.

116. Livak, K.J. and Schmittgen, T.D. (2001). Analysis of relative gene expression data using real-time quantitative PCR and the 2(-Delta Delta C(T)) Method. Methods *25*, 402-408.

117. Schneider, C.A., Rasband, W.S., and Eliceiri, K.W. (2012). NIH Image to ImageJ: 25 years of image analysis. Nat. Methods *9*, 671-675.

bioRxiv preprint doi: https://doi.org/10.1101/2025.02.02.636139; this version posted February 6, 2025. The copyright holder for this preprint (which was not certified by peer review) is the author/funder, who has granted bioRxiv a license to display the preprint in perpetuity. It is made available under aCC-BY-NC-ND 4.0 International license.

STAR★METHODS (full online version)

KEY RESOURCES TABLE:

REAGENT or RESOURCE	SOURCE	IDENTIFIER
Antibodies		
anti-β-actin, HRP-conjugated mouse monoclonal antibody (1:50,000 dilution)	Millipore-Sigma	Catalog # A3854 RRID:AB_262011
anti-AKT1, rabbit monoclonal antibody (1:1,000 dilution)	Cell Signaling	Catalog # 2938 RRID:AB_915788
anti-phospho-AKT1 (Ser473), rabbit monoclonal antibody (1:1,000 dilution)	Cell Signaling	Catalog # 9018 RRID:AB_2629283
anti-ERK1/2, rabbit polyclonal antibody (1:1,000 dilution)	Cell Signaling	Catalog # 9102 RRID:AB_330744
anti-phospho-ERK1/2 (Thr202/Tyr204), rabbit polyclonal antibody (1:1,000 dilution)	Cell Signaling	Catalog # 9101 RRID:AB_331646
anti-cJun, rabbit monoclonal antibody (1:1,000 dilution)	Cell Signaling	Catalog # 9165 RRID:AB_2130165
anti-phospho-cJun (Ser73), rabbit monoclonal antibody (1:1,000 dilution)	Cell Signaling	Catalog # 3270 RRID:AB_2129575
anti-LRRC8A, mouse monoclonal antibody (1:1,000 dilution)	Santa Cruz Biotech.	Catalog # sc-517113 RRID:AB_2928142
anti-S6 Ribosomal Protein, rabbit monoclonal antibody (1:1,000 dilution)	Cell Signaling	Catalog # 2217 RRID:AB_331355
anti-phospho-S6 Ribosomal Protein (Ser240/244), rabbit monoclonal antibody (1:1,000 dilution)	Cell Signaling	Catalog # 5364 RRID:AB_10694233
anti-SPAK, rabbit polyclonal antibody (1:1,500 dilution)	Cell Signaling	Catalog # 2281 RRID:AB_2196951
anti-phospho-SPAK/OSR (Ser373/325), rabbit polyclonal antibody (1:1,500 dilution)	Millipore-Sigma	Catalog # 07-2273 RRID:AB_11205577
donkey anti-rabbit IgG, HRP-conjugated (1:10,000 dilution)	GE Healthcare	Catalog # NA932
sheep anti-mouse IgG, HRP-conjugated (1:10,000 dilution)	GE Healthcare	Catalog # NA931
qPCR Primers		
RPL13a (housekeeping) Hs_RPL13A_1_SG	Qiagen	GeneGlobe ID QT00089915
RPS20 (housekeeping) Hs_RPS20_1_SG or Hs_RPS20_2_SG	Qiagen	QT00003290; QT01666847
GAPDH (housekeeping) Hs_GAPDH_1_SG or Hs_GAPDH_2_SG	Qiagen	QT00079247; QT01192646
GFAP Hs_GFAP_1_SG	Qiagen	QT00081151
LRRC8A Hs_LRRC8A_1_SG	Qiagen	QT01023302
LRRC8B Hs_LRRC8B_1_SG	Qiagen	QT01017450
LRRC8C Hs_LRRC8C_1_SG	Qiagen	QT00055720
LRRC8D Hs_LRRC8D_2_SG	Qiagen	QT01679202

bioRxiv preprint doi: https://doi.org/10.1101/2025.02.02.636139; this version posted February 6, 2025. The copyright holder for this preprint (which was not certified by peer review) is the author/funder, who has granted bioRxiv a license to display the preprint in perpetuity. It is made available under aCC-BY-NC-ND 4.0 International license.

LRRC8E Hs_LRRC8E_1_SG	Qiagen	QT00079639
WNK1 Hs_WNK1_1_SG	Qiagen	QT00085939

siRNA constructs

AllStars Negative Control siRNA (siNC) (target sequence proprietary)	Qiagen	GeneGlobe ID SI03650318
Hs_LRRC8A_3 (target seq. CTGCCTTAAGCTGTGGTACAA)	Qiagen	SI04251807
Hs_LRRC8A_4 (target seq. GACGGGCGTGCTGGACAAGAA)	Qiagen	SI04327001
Hs_LRRC8A_5 (target seq. CTGCGTCGTGTCATTGGATAT)	Qiagen	SI05006029
Hs_LRRC8A_6 (target seq. CAGGGTGGCAGTTTCCCTTGA)	Qiagen	SI05006036
Hs_WNK1_5 (target seq. CTAGAGGATCTTGATGCTCAA)	Qiagen	SI00288547
Hs_WNK1_6 (target seq. CTGCGACGACTACGAGATAAA)	Qiagen	SI02622389
Hs_WNK1_12 (target seq. CAGAAAGTTCTGTTTCGGGAA)	Qiagen	SI05104176

Chemicals

D-[2,3-^{3}H]aspartate	PerkinElmer/Revvity	Catalog # NET50100
Chlorine-36 (chemical form: sodium chloride)	American Radio-labeled Chemicals	Catalog # ARX0104
L-[3,4-^{3}H]glutamic acid	PerkinElmer/Revvity	Cat# NET490250UC
Anisomycin	Tocris Bioscience	Catalog #1290 CAS 22862-76-6
BSJ-04-122 (MKK4/7 inhibitor)	MilliporeSigma	Catalog # SML3061 CAS 2513289-74-0
BSJ-04-122R (inactive analog of BSJ-04-122)	MilliporeSigma	Catalog # SML3062 CAS 2513289-75-1
G□-6976 (inhibitor of conventional PKCs)	Selleck Chemicals	Catalog # S7119 CAS 136194-77-9
GSK650394 (SGK inhibitor)	Santa Cruz Biotech.	Catalog # sc-361201 CAS 890842-28-1
KU0063794 (mTORC1/2 inhibitor)	Tocris Bioscience	Catalog # 3725 CAS 938440-64-3
Lipofectamine RNAiMAX Transfection Reagent	Thermo Fisher Sci.	Catalog # 13778075
MK-2206 dihydrochloride (AKT inhibitor)	Cayman Chemical	Catalog # 11593 CAS 1032350-13-2
MTT (Thiazolyl Blue Tetrazolium Bromide)	Millipore-Sigma	Catalog # M2128 CAS 298-93-1
PI 828 (PI3K inhibitor)	Tocris Bioscience	Catalog # 2814 CAS 942289-87-4
SP600125 (JNK inhibitor)	Tocris Bioscience	Catalog # 1496 CAS 129-56-6

bioRxiv preprint doi: https://doi.org/10.1101/2025.02.02.636139; this version posted February 6, 2025. The copyright holder for this preprint (which was not certified by peer review) is the author/funder, who has granted bioRxiv a license to display the preprint in perpetuity. It is made available under aCC-BY-NC-ND 4.0 International license.

U-0126 (MEK1/2 inhibitor)	Tocris Bioscience	Catalog # 1144 CAS 109511-58-2
WNK463 (WNK inhibitor)	Selleck Chemicals	Catalog # S8358 CAS# 2012607-27-9

Critical commercial assays

Aurum Total RNA Mini Kit	Bio-Rad	Catalog # 7326820
ECL Prime reagent	GE Healthcare	Catalog # RPN2232
ECL Clarity reagent	Bio-Rad	Catalog # 1705061
iScript cDNA Synthesis Kit	Bio-Rad	Catalog # 1708891
iQ SYBR Green Supermix	Bio-Rad	Catalog # 1708882
LDH-Glo Cytotoxicity Assay	Promega	Catalog # J2380
Mycoplasma PCR Detection Kit	Abcam	Catalog # ab289834
Pierce Bicinchoninic Acid assay	Thermo Fisher Sci.	Catalog # 23225

Other reagents and components

DMEM, minimal essential medium, high glucose	Thermo Fisher Sci.	Catalog # 11965118
Ecoscint A scintillation cocktail	National Diagnostics	Catalog # LS-273
Fetal Bovine Serum, qualified	Thermo Fisher Sci.	Catalog # 26140079
G5 Supplement	Thermo Fisher Sci.	Catalog # 17503012
Halt Phosphatase inhibitor cocktail	Thermo Fisher Sci.	Catalog # 78430
Halt Protease inhibitor cocktail	Thermo Fisher Sci.	Catalog # 87786
Laemmeli Sample buffer (2X)	Bio-Rad	Catalog # 1610737
Mini-PROTEAN precast protein gels (10%)	Bio-Rad	Cat # 4561034DC
Precision Plus Protein Dual Color Standard	Bio-Rad	Catalog # 1610374
TrypLE express, recombinant protease	Thermo Fisher Sci.	Catalog # 12605010

Experimental models: Cell lines

Human astrocytes (several independent batches)	ScienCell Research Laboratories	Catalog # 1800
Patient-derived glioblastoma cells, GBM1	This study	GBM1
Patient-derived glioblastoma cells, GBM8	This study	GBM8

Normal brain RNA sources:

FirstChoice Total RNA, Human Brain	Thermo Fisher Sci.	Catalog # AM7962
Total RNA, Human Brain	Takara Bio	Catalog # 636530
Total RNA, Human Brain, Cerebral Cortex	Takara Bio	Catalog # 636561

Software, algorithms, and publicly available datasets

Bioconductor version 3.18	Bioconductor	RRID:SCR_006442
DESeq2 version 1.42.0	Bioconductor	RRID:SCR_015687
dplyr version 1.1.4	R Project	RRID:SCR_016708
ggplot2 version 3.5.1	R Project	RRID:SCR_014601
GraphPad Prism version 10.3	GraphPad Software	RRID:SCR_002798
ImageJ version 1.53u	National Institutes of Health	RRID:SCR_003070
R Project for Statistical Computing version 4.4.0	R Project	RRID:SCR_001905
RStudio version 2023.12.1+402	Posit Software	RRID:SCR_000432

bioRxiv preprint doi: https://doi.org/10.1101/2025.02.02.636139; this version posted February 6, 2025. The copyright holder for this preprint (which was not certified by peer review) is the author/funder, who has granted bioRxiv a license to display the preprint in perpetuity. It is made available under aCC-BY-NC-ND 4.0 International license.

SummarizedExperiment version 1.32.0	Bioconductor	doi:10.18129/B9.bioc.SummarizedExperiment
survival 3.6-4	R Project	RRID:SCR_021137
survminer version 0.4.9	Rdocumentation.org	RRID:SCR_021094
TCGAbiolinks version 2.30.0	Bioconductor	RRID:SCR_017683
The Cancer Genome Atlas	National Institutes of Health	RRID:SCR_003193
tidyverse version 1.3.0	R Project	RRID:SCR_019186

Hardware

ChemiDoc Imager	Bio-Rad	RRID:SCR_019684
Olympus IX71 S8F-3 Microscope	Olympus Corp.	RRID:SCR_022185
Spectra/Chrom CF-1	SpectraLab Sci.	Cat. # SPE-CF-1
Tri-Carb 4910TR Scintillation Counter	PerkinElmer/Revvity	N/A
Victor Nivo Multimode Plate Reader	PerkinElmer/Revvity	Cat. # HH35000500

RESOURCE AVAILABILITY

Lead contact

Further information and requests for resources and reagents should be directed to and will be fulfilled (as available) by the Lead Contact, Alexander A. Mongin.

Materials and availability statement

Due to the very limited amount of surgery derived GBM specimens, there are restrictions to the availability of GBM-derived cDNA and protein samples. Early passages of primary GBM cells are not available due to their scarcity. This study has used and validated unique molecular biology tools that are fully described in Key Resources Table and available from commercial sources. All primary data derived from this work are freely available as specified below.

Data and code availability

- All patient samples used in this study have been deidentified
- All primary data used for analyses in this work are deposited in the Open Science Framework (osf.io) and are freely accessible for re-analysis at https://osf.io/2r7k9
- Original R codes used in the analysis of TCGA materials are deposited in the Open Science Framework and accessible at https://osf.io/sfvjg/ (TPM expression analysis) and https://osf.io/q6mvz (DEseq2-based patient survival analysis).

EXPERIMENTAL MODEL AND STUDY PARTICIPANTS DETAILS

Patient samples

Human GBM specimens were collected from 28 patients diagnosed with glioblastoma (WHO grade IV) and operated in the Department of Neurosurgery at Albany Medical Center System Hospital (AMCSH), Albany, New York, USA. The glioblastoma origin of tissue samples was

bioRxiv preprint doi: https://doi.org/10.1101/2025.02.02.636139; this version posted February 6, 2025. The copyright holder for this preprint (which was not certified by peer review) is the author/funder, who has granted bioRxiv a license to display the preprint in perpetuity. It is made available under aCC-BY-NC-ND 4.0 International license.

confirmed during surgical resection by the standard histopathology in the Department of Pathology at AMCSH. The unused GBM tissue samples were collected in a sterile container filled with ice-cold saline, deidentified, and transferred on ice to further processing in a molecular biology laboratory. There, specimens were dissected from heavily vascularized parts by a sharp scalpel and separated into three parts for isolation of cDNA, generation of protein lysates, and preparation of primary glioblastoma cells as described below. All relevant procedures were approved by the Institutional Review Board of Albany Medical College (IRB # 2536, 6006). Written informed consent was obtained from the patients or their authorized representatives in accordance with the Declaration of Helsinki[115] (rev.2024 https://www.wma.net/policies-post/wma-declaration-of-helsinki/, last accessed on 11/11/2024).

Patient-derived primary GBM cell lines

GBM tissue specimens were washed in an ice-cold sterile phosphate-buffered saline (PBS), transferred into a Petri dish and cut into smaller fragments with a scalpel. Dissected tissue was further digested in the solution of 0.125% trypsin plus 0.015% EDTA for 10 minutes at 37^{o}C. Cells were dissociated by mechanical trituration using a fire-polished glass Pasteur pipette, and the resulting suspension was filtered through a 70-µm cell strainer (Corning). Protease activity was quenched by adding an excess of Optimized Minima Essential Medium (Opti-MEM, Thermo Fisher Scientific) which was supplemented with 10% fetal bovine serum (FBS, Thermo Fisher Scientific), 100 U/ml penicillin and 100 µg/ml streptomycin (pen-step, Thermo Fisher Scientific). The final cell suspension was plated in a 75 cm^2 flask (T75, Corning) and cultivated in a CO_2 incubator in a mixture of 5% CO_2/balance air at 37^{o}C. After cells adhered to plastic, medium was replaced with high glucose Dulbecco's Modified Eagle's Medium (DMEM, Thermo Fisher Scientific) supplemented with 10% FBS and pen-step. Medium was fully replaced twice a week and GBM cell cultures were grown to ~90% confluency. For propagation, cells were removed from a substrate using the recombinant protease TrypLE (Thermo Fisher Scientific) and replated into T75 or cryoprotected. Initial gene expression analyses were performed in passages 1 or 2. For all other described in this study experiments, GBM cells were used before passage 10 (in majority of cases at passages 4-6).

Human GBM datasets in The Cancer Genome Atlas (TCGA)

We downloaded from TCGA (https://www.cancer.gov/ccg/research/genome-sequencing/tcga) all publicly available GBM datasets matching the following criteria: (i) identified as GBM, non-mutant (wild-type) isocitrate dehydrogenase (IDH1/2), (ii) complete RNAseq available, (iii) survival data available. Altogether, we analyzed data from 126 patients of both sexes (see Results section and additional information below). The healthy brain controls were sourced from the Gene Expression Omnibus repository and represent 29 brains (GEO series GSE196695).

METHOD DETAILS

Computational analysis of glioblastoma databases in TCGA

bioRxiv preprint doi: https://doi.org/10.1101/2025.02.02.636139; this version posted February 6, 2025. The copyright holder for this preprint (which was not certified by peer review) is the author/funder, who has granted bioRxiv a license to display the preprint in perpetuity. It is made available under aCC-BY-NC-ND 4.0 International license.

Publicly available GBM datasets were downloaded from TCGA and processed using an open-source programming language R (version 4.3.1), the R Studio platform (v. 2023.12.1+402), and the R package TCGAbiolinks (v. 2.30.0). The R codes used in our analyses have been deposited in the Open Science Framework, as referenced in the *Data and Code Availability* section. For comparisons of relative expression of multiple LRRC8 genes (LRRC8A-E) across GBM and normal brain tissue specimens, RNAseq data were downloaded and analyzed as transcript per million (TPM) counts. For additional survival analysis, patient LRRC8A RNAseq levels were downloaded as unstranded counts and normalized using the DEseq2 variance-stabilizing transformation. The latter normalization is considered superior to TPM and FPKM for comparisons of individual gene expression because it accounts for sample-to-sample differences in library size, sequencing depth, and expression profile.[59,60] For survival analysis patients were separated into four quartiles and statistically compared using the Kaplan-Meier method (see *Statistical analyses*).

mRNA isolation and real-time quantitative PCR

mRNA was extracted from tumor tissue or GBM cultures using the Aurum Total RNA Mini Kit (Bio-Rad Laboratories). Briefly, 100-300 mg of tissue was carefully dissected in a Petri dish using scalpel and forceps pretreated in diethylpyrocarbonate (DEPC) and lysed using the lysis buffer provided with a kit. In cell preparations, GBM cells were additionally washed from culture medium with Ca^{2+}/Mg^{2+}-containing PBS prior lysis. Lysates were homogenized by pipetting, mixed with equal parts ice-cold 70% EtOH and processed per manufacturer's protocol. RNA concentrations were measured using the NanoDrop 1000 spectrophotometer (Thermo Fisher Scientific). Subsequent cDNA generation was done using the iScript cDNA synthesis kit (Bio-Rad Laboratories) using one µg of RNA per each 20 µLs of reaction volume. Resulting cDNA samples were aliquoted and stored at –80^{o}C. mRNA expression levels were assessed by quantitative real-time PCR (qRT-PCR) in a CFX96 Real Time System (Bio-Rad) with validated quantitative PCR primers (Qiagen, see the Key Resourses Table) and SYBR Green Master Mix (Bio-Rad). Expression levels were calculated by the ΔCt (for tissue and cell expression) or ΔΔCt method[116] (in RNAi analyses). Data were normalized within the sample to the housekeeping gene RPL13a. GAPDH and RPS20 were probed as additional housekeeping and quality controls.

Protein isolation and Western blotting analysis

Proteins were extracted from tumor tissue samples or cell cultures by lysis in the solution of 2% SDS plus 8 mM EDTA, additionally containing Halt phosphatase and protease inhibitors (Thermo Fisher Scientific). A small aliquot of each lysate was used for determining protein content using the Pierce Bicinchoninic acid protein assay kit (Thermo Fisher Scientific). The remaining lysates were mixed with 2× reducing Laemmli buffer (Bio-Rad), aliquoted, and stored at −80^{o}C until analysis. 20-µg protein samples were loaded on precast 10% acrylamide gels (Bio-Rad), separated using SDS-PAGE, and subsequently transferred onto PVDF membrane (Bio-Rad) using a Trans-Blot Turbo transfer system (Bio-Rad). Membranes were next blocked for 15 min in either 5% fat-free milk or EveryBlot Blocking Buffer (Bio-Rad, used for all phosphoprotein analyses) and incubated with primary antibodies overnight at 4^{o}C. After several

bioRxiv preprint doi: https://doi.org/10.1101/2025.02.02.636139; this version posted February 6, 2025. The copyright holder for this preprint (which was not certified by peer review) is the author/funder, who has granted bioRxiv a license to display the preprint in perpetuity. It is made available under aCC-BY-NC-ND 4.0 International license.

washes, membranes were additionally incubated with an appropriate HRP-conjugated secondary antibody for 90-min at room temperature. Chemiluminescence signal of proteins of interest was captured using the ChemiDoc MP Imaging System (Bio-Rad) and quantified using an ImageJ software[117] (National Institute of Health, v. 1.53u). To ensure equal protein load, one-to-two days after initial western blotting, membranes were re-probed without stripping with the HRP-conjugated antibody recognizing the housekeeping protein β-actin. Protein levels were normalized to housekeeping protein signal, and further double normalized to average immunofluorescence in at least two 'control' samples on the same Western blot membrane (e.g., 'control siRNA' or 'vehicle treated'). In assays measuring phosphospecific protein signal, immunoluminescence values were additionally analyzed by dividing normalized phosphoprotein signal by normalized total protein signal in the same lysate. (all antibodies and their dilution factors are listed in *Key Resources Table*).

siRNA manipulation of gene expression

siRNA transfections were carried out using Lipofectamine RNAiMAX reagent (Thermo Fisher Scientific) following the manufacturer's recommendations. In short, siRNA/Lipofectamine RNAiMAX complexes were prepared in Opti-MEM, in a light-protected environment, and then added to cell cultures bathed in a serum-free Opti-MEM. The final siRNA concentration was 10, 25, of 50 nM (optimized for each construct). After an initial 4-h incubation, Opti-MEM was supplemented with DMEM containing 10% FBS and 0.5% penicillin-streptomycin. The efficacy of siRNA constructs was measured 48-h after transfection using qRT-PCR (see the Key Resources Table for the list of siRNA constructs and target sequences). Protein isolation and functional assays were performed 96-hours after transfection.

Radiotracer assays of VRAC activity

Activity of VRAC was quantified by measuring the release of the radiolabeled VRAC-permeable, non-metabolizable analog of glutamate D-[^{3}H]aspartate. GBM cells or primary human astrocytes were grown to confluency on 18-mm square coverslips and subsequently treated with siRNA as indicated. After 72 h, cells were additionally incubated overnight with 2 µCi/ml D-[^{3}H]aspartate (PerkinElmer) in DMEM+10% FBS in a CO_2 incubator at 37^{o}C. The next day, cells were washed from intracellular isotope with warm chemically defined isoosmotic Basal medium containing (in mM) 135 NaCl, 3.8 KCl, 1.2 $MgSO_4$, 1.3 $CaCl_2$ mM, 1.2 KH_2PO_4, 10 D-glucose, and 10 HEPES (pH 7.4, osmolarity 290 ±3 mOsm). Coverslips were loaded in a Lucite perfusion chamber with Teflon top that leaves approximately 200-300 µm above coverslip, and superfused at the rate of ~1.2 ml/min with either isoosmotic Basal medium or hypoosmotic medium. The composition of hypoosmotic medium was similar with the exception that NaCl concentration was reduced to 85 mM leading to a 30% decrease in medium osmolarity (190 ±3 mOsm, verified by a freezing point micro-osmometer µOsmette, Precision Systems, Natick, MA, USA). One-minute perfusate fractions were collected using an automated fraction collector (Spectra/Chrom CF-1, SpectraLab, Markham, ON, Canada). Individual superfusate fractions were next mixed with an Ecoscint A scintillation cocktail (National Diagnostics, Atlanta, GA, USA), and the levels of released D-[^{3}H]aspartate in each sample were determined using a Tri-Carb 4910TR scintillation counter (PerkinElmer). To determine the amount of radiotracer remaining inside cells on a coverslip, after completion of experiment, cells were lysed in the solution of 2% SDS plus 8mM EDTA. Fractional isotope release rates were calculated using an Excel-based custom algorithm.

bioRxiv preprint doi: https://doi.org/10.1101/2025.02.02.636139; this version posted February 6, 2025. The copyright holder for this preprint (which was not certified by peer review) is the author/funder, who has granted bioRxiv a license to display the preprint in perpetuity. It is made available under aCC-BY-NC-ND 4.0 International license.

Measurements of intracellular Cl levels

Intracellular chloride levels were analyzed by measuring steady-state accumulation of the radiotracer $^{36}Cl^-$. Cells were grown to confluency in six-well plates, in DMEM+10% FBS in the atmosphere containing 5% CO_2/balance air at 37^{o}C. Confluent cells were equilibrated overnight in Opti-MEM +10% FBS. To initiate isotope uptake, an aliquot of Opti-MEM+FBS additionally containing $^{36}Cl^-$ (American Radiolabeled Chemicals) was added to each well to the final isotope activity 0.5 µCi/ml. After 20-min incubation, isotope uptake was terminated by washing four times with an ice-cold solution containing (in mM) 300 D-mannitol, 1.2 $MgSO_4$, and 10 HEPES (pH 7.4, 320 ± 3 mOsm). After the final wash, cells were lysed in 2% SDS plus 8 mM EDTA. Cell lysates were mixed with the scintillation cocktail Ecoscint A (National Diagnostics) and intracellular $^{36}Cl^-$ levels were determined using a Tri-Carb 4910TR scintillation counter (Revvity). $^{36}Cl^-$ radioactivity was further normalized to protein levels in each well.

Cell proliferation assays

Cellular proliferation was measured using the MTT proliferation assay. Cells were plated at low densities (15K/well for GBM1 or 30K/well for GBM8) and allowed to adhere overnight. Cells were then transfected with siRNA (see above) or treated with pharmacological inhibitors as indicated in figure legends. After 4 days of transfection or 3 days of pharmacological treatments, cell culture media were washed with isoosmotic Basal medium and incubated in the Basal medium containing 0.5 mg/ml MTT for 1-2 hours at 37^{o}C. MTT-containing media were removed, and the newly formed intracellular formazan crystals were solubilized with dimethyl sulfoxide (DMSO). The optical density of the formazan solutions were determined by measuring the absorbance at 562 nm in an ELx800 plate reader (BioTek). Data are presented as the percentage of MTT signal compared to within-plate untreated or negative control cells.

In addition, DAPI-stained nuclei counting was used as an alternative method to ascertain the effect of certain treatments on cell proliferation. Cells were plated and treated as described above. On the final day, cell culture medium was aspirated, and cells were fixed in 4% paraformaldehyde in PBS for 15 minutes at room temperature (22-23^{o}C). 4% PFA/PBS solution was aspirated, wells were gently washed twice with cold Ca^{2+}/Mg^{2+}-free DPBS and incubated in ice-cold DPBS containing 300 nM DAPI for 20 minutes at room temperature in a light-protected environment. DAPI-stained nuclei were imaged at 10× magnification using a Keyence BZ-X800 fluorescent microscope (Keyence Corporation) and counted using ImageJ.

Fluorescence-assisted cell sorting (FACS) analysis of cell cycle stage

Cellular DNA content was determined by staining cells with propidium iodide and measuring fluorescence using a Becton Dickinson FACScan (Rutherford, NJ, USA). Cells were harvested by trypsinization and fixed in cool 70% ethanol for 6 h. Subsequently, fixed cells were incubated in a solution containing 1 mg/ml RNase and 20 µg/ml propidium iodide for 30 min. For each cell population, 10,000 cells were analyzed by FACS and the proportion of cells in G_0/G_1, S, and G_2/M phases was measured estimated using the FlowJo program (version 10.0).

bioRxiv preprint doi: https://doi.org/10.1101/2025.02.02.636139; this version posted February 6, 2025. The copyright holder for this preprint (which was not certified by peer review) is the author/funder, who has granted bioRxiv a license to display the preprint in perpetuity. It is made available under aCC-BY-NC-ND 4.0 International license.

Cell death assay

Cell death was assessed by measuring levels of lactate dehydrogenase (LDH) release using a luciferase reporter-based LDH cytotoxicity assay (LDH-Glo, Promega Corporation). To reduce contribution of nonspecific LDH signal originating from FBS, cells were grown in Opti-MEM plus G5 serum-free supplement. After 1, 3, or 4 days, cell culture media from each well was sampled, mixed with equal parts of LDH storage buffer, and transferred onto ice. The remaining cells were lysed in LDH lysis buffer. Cell lysates were further diluted in an LDH storage buffer and kept on ice. Supernatants and cell lysates were transferred into 96-well plates, mixed with a freshly prepared detection reagent, and levels of luminosity were measured using a Victor Nivo 3T Multimode Plate Reader (Revvity). As a positive control for cell death, cells were treated with the protein kinase inhibitor staurosporine (STS; 300nM, 24-hours prior to processing). Relative LDH release levels were calculated by dividing the background-corrected LDH signal in supernatants by the total LDH levels in cell lysates from the same wells. Cell death values are reported as percentages.

QUANTIFICATION AND STATISTICAL ANALYSIS

All data are presented as the mean values ±SD, with the number of independent experiments (n) indicated in each figure. n represents an independently prepared and treated cell culture, or an individual patient in human datasets. Experimental data were tested for normal distribution. In most cases, statistical differences between groups with normal distribution were determined by one-way ANOVA with Dunnett's post hoc correction for multiple comparisons. The two-group comparisons were done using an unpaired t-test. In those instances where data were normalized to within-experiment controls, statistical comparisons were performed using a one-sample t-test with the Bonferroni correction. Gene expression data were compared using an unpaired t-test with the Welch correction and Holm-Šídák adjustment. The survival rates for GBM patients were compared using the Gehan-Breslow-Wilcoxon test. Plotting and statistical analyses were done using Prism software (version 10.3.0, GraphPad Software).

bioRxiv preprint doi: https://doi.org/10.1101/2025.02.02.636139; this version posted February 6, 2025. The copyright holder for this preprint (which was not certified by peer review) is the author/funder, who has granted bioRxiv a license to display the preprint in perpetuity. It is made available under aCC-BY-NC-ND 4.0 International license.

FIGURE LEGENDS

Figure 1. LRRC8A is upregulated in human GBM specimens and patient-derived GBM cultures and promotes cell proliferation

(**A1**) *Lrrc8* mRNA expression levels in surgically resected GBM tumor specimens (n=22) and healthy brain tissue (3 RNA medleys from 8 brains) measured using qRT-PCR and normalized to the housekeeping gene *Rpl13a*. ***p<0.001, GBM vs. normal brain.

(**A2**) Comparison of *Lrrc8* mRNA expression levels in patient derived GBM cell cultures (n=12) and primary human astrocytes (n=6). *p<0.05, **p<0.01, ***p<0.001, GBM vs. astrocytes.

(**A3**) In-silico analysis of RNA-seq data for the expression of *Lrrc8* isoforms in primary GBM (n=126) and healthy brain tissue (3 RNA medleys from 29 brains). GBM expression values were obtained from TCGA. Healthy brain tissue data were sourced from GEO repository, series GSE196695. ****p<0.0001, GBM vs. normal brain.

In A1-A3, data are presented as boxplots with individual values and compared with an unpaired t-test with Welch correction and Holm-Šídák adjustment.

(**B**) Representative images of the patient-derived GBM1 (*LEFT*) and GBM8 (*RIGHT*) cells. Images were acquired using Hoffman optics at identical 160× magnification.

(**C**) VRAC activity in GBM1, GBM8, and primary human astrocytes measured as swelling activated release of preloaded D-[^{3}H]aspartate. Cell swelling was induced by 30% reduction in medium osmolarity (HYPO). Mean values ±SEM from 4-6 independent experiments/cell line.

(**D1**) Representative western blot image probing downregulation of LRRC8A in GBM1 and GBM8 cells treated with the LRRC8A-specific siRNAs, siA3 and siA5, and compared to the negative control siRNA (siNC). Lower inset shows the same membrane re-probed for β-actin immunoreactivity.

(**D2**) Quantification of LRR8A expression in siRNA-treated GBM cultures. Mean values ±SD from 5 independent transfections/cell line. One-sample t-test with Bonferroni's correction. ****p<0.0001 vs siNC.

(**E**) Functional downregulation of VRAC activity in GBM1 cells treated with LRRC8A siRNA (siA5) and compared to siNC. Mean values ±SEM (n=5/condition). ***p<0.001 vs. siNC, t-test comparing integral D-[^{3}H]aspartate release values during hypotonic exposure.

(**F**) Effect of LRRC8A knockdown with the LRRC8A-specific siRNAs siA3 and siA5 on relative proliferation in GBM1 and GBM8 measured using the MTT assay. Mean values ±SD from 8-10 independent transfections. One-sample t-test with Bonferroni's correction, ****p<0.0001 vs. siNC.

Figure 2. In-silico analysis of the relationship between *Lrrc8a* mRNA expression and life expectancy in GBM patients

(**A**) In-silico analysis of RNA-seq expression for *Lrrc8a* in primary GBM tissues (n=126) separated into quartiles. Data were sourced from TCGA and normalized using the DEseq2 variance-stabilizing transformation. Expression values presented as boxplots with individual values.

(**B**) Kaplan-Meier plot of survival rates for GBM patients grouped by tumor *Lrrc8a* expression quartile. Median survival was compared between the lowest (Q1; n=27) and highest (Q4; n=27) *Lrrc8a* expressers using the Gehan-Breslow-Wilcoxon test. p=0.078.

Figure 3. Analysis of functional interactions between LRRC8A and GRB2-dependent growth factor signaling pathways in GBM

bioRxiv preprint doi: https://doi.org/10.1101/2025.02.02.636139; this version posted February 6, 2025. The copyright holder for this preprint (which was not certified by peer review) is the author/funder, who has granted bioRxiv a license to display the preprint in perpetuity. It is made available under aCC-BY-NC-ND 4.0 International license.

(**A**) Diagram depicting receptor tyrosine kinase (RTK)-ERK1/2 signaling pathway and its putative interactions with LRRC8A. For abbreviations and further information see text.

(**B,C,E**) Western blot analysis of the effect of LRRC8A downregulation on ERK1/2 signaling in GBM1 cells. Representative images and quantification of phospho-ERK1/2 (**B1-B2**), total ERK1/2 (**C1-C2**), and phospho/total ERK1/2 immunoreactivity ratio (**E**). GBM1 cells were treated with the LRRC8A-specific siRNAs, siA3 and siA5, and compared to the negative control siNC (n=9). GBM1 cells treated with the ERK1/2 inhibitor Trametinib (Tram; 0.3 μM, 6-hr) and non-transfected cells (NTF) were included as additional controls (n=6-8). Data are the mean values ± SD. One-way ANOVA with Dunnett's correction, ****p<0.0001, trametinib vs siNC.

(**D**) Effect of the ERK1/2 signaling inhibitor U-0126 (ERKi; 10μM) on GBM1 and GBM8 proliferation as compared to vehicle control (Veh; 0.1% DMSO). Cell proliferation values were measured using the MTT assay and normalized to within-plate untreated cells (n=6/cell line). Data are the mean values ± SD. ns, not significant, unpaired t-test.

(**F**) Diagram depicting RTK-JNK signaling pathway and its putative interactions with LRRC8A. For abbreviations and further information see text.

(**G,H,J**) Western blot analysis of the effect of LRRC8A downregulation on JNK signaling in GBM1 cells using cJun phosphorylation as a readout. Representative images and quantification of phospho-cJun (**G1-G2**), total cJun (**H1-H2**), and phospho/total cJun immunoreactivity ratio (**J**) in GBM1 cells treated with the LRRC8A-specific siA3 and siA5 as compared to siNC. As controls, GBM1 were treated with the JNK inhibitor SP600125 (SP, 20 μM, 24-hr), the MKK4/7 inhibitor BSJ-04-122 (BSJ, 5μM, 24-hr), or the JNK activator anisomycin (Aniso; 10μM, 2-hr). Data are the mean values ± SD from 6 siRNA experiments and 3-4 pharmacological controls. One-way ANOVA with Dunnett's correction, *p<0.05, **p<0.01, ***p<0.001, ****p<0.0001 vs. siNC.

(**I**) Effect of the JNK signaling inhibitor SP600125 (JNKi, 20μM) on GBM1 and GBM8 proliferation. The MTT assay values were normalized to within-plate untreated cells and compared to the vehicle control (Veh; 0.1% DMSO). Data are the mean values ± SD (n=6-8/cell line). Unpaired t-test, ****p<0.0001 vs. Veh.

Figure 4. Analysis of functional interactions between LRRC8A and the GRB2-dependent PI3K/AKT/mTORC1 signaling axis in GBM

(**A**) Diagram depicting RTK-PI3K/AKT/mTORC1 signaling axis and its putative interactions with LRRC8A. For abbreviations and further information see text.

(**B,C,E**) Western blot analysis of the effect of LRRC8A downregulation on mTORC1 signaling in GBM, measuring S6 phosphorylation as a readout. Representative images and quantification of phospho-S6 (**B1-B2**), total S6 (**C1-C2**), and phospho/total S6 immunoreactivity ratio (**E**). GBM1 cells were treated with the LRRC8A-specific siRNAs, siA3 and siA5, or the negative control siNC. As controls, cells were treated with the mTORC1 inhibitor Rapamycin (Rap, 10nM, 48-hr), or the mTORC1/2 blocker KU-0063794 (KU, 2.5 μM, 48-hr). NTF, non-transfected cells. Data are the mean values ± SD from 6 siRNA transfections or 2-3 pharmacological controls. One-way ANOVA with Dunnett's correction, **p<0.01, ***p<0.001 vs. siNC.

(**E**) Effect of the PI3K signaling inhibitor PI 828 (PI3Ki, 2.5μM) on GBM1 and GBM8 proliferation. The MTT assay values were normalized to within-plate untreated cells and compared to the vehicle control (Veh; 0.1% DMSO). Data are the mean values ± SD (n=6-7/cell line). Unpaired t-test, **p<0.01, ****p<0.0001 vs. Veh.

Figure 5. Effect of LRRC8A knockdown on $[Cl^-]_i$ and the Cl^--sensitive WNK signaling axis

bioRxiv preprint doi: https://doi.org/10.1101/2025.02.02.636139; this version posted February 6, 2025. The copyright holder for this preprint (which was not certified by peer review) is the author/funder, who has granted bioRxiv a license to display the preprint in perpetuity. It is made available under aCC-BY-NC-ND 4.0 International license.

(**A**) Kinetics of $^{36}Cl^-$ accumulation in GBM1 cells measured in a serum-containing cell culture medium. Data are the mean values ± SD of 4 independent assays.
(**B**) Effect of LRRC8A knockdown on a steady state $^{36}Cl^-$ accumulation in GBM1 cells. Cells were transfected with the LRRC8A-specific siRNAs, siA3 and siA5, or the negative control siNC. 96-h later, intracellular Cl^- levels were measured as steady state $^{36}Cl^-$ uptake. Data are the mean values ± SD from 8 independent transfections. One-way ANOVA with Dunnett's correction. **p<0.01, ****p<0.0001 vs. siNC.
(**C**) Effect of the putative VRAC blocker DIDS (500 µM) on GBM1 and GBM8 cell proliferation as compared to untreated cells (WT). Proliferation was quantified using an MTT assay and normalized to untreated cells on the same plate. Data are the mean ±SD. n=4-10/cell line. One-sample t-test. *p<0.05, ****p<0.0001 vs WT.
(**D,E,G**) Western blot analysis of the effect of LRRC8A downregulation on WNK signaling in GBM1, measured using SPAK phosphorylation as a readout. Representative images and quantification of phospho-SPAK (**D1-D2**), total SPAK (**E1-E2**), and phospho/total SPAK immunoreactivity ratio (**G**). GBM1 were treated with the LRRC8A-specific siA3 and siA5 or the negative control siNC (n=9). As controls, cells were treated with the WNK inhibitor WNK463 ('WNKi', 1µM, 24-hr) or hyperosmotic medium supplemented with 300 mM mannitol ('Mann', 1-hr treatment). NTF, non-transfected cells. n=4-6 for pharmacological controls. Data are the mean ±SD. One-way ANOVA with Dunnett's correction, *p<0.05, **p<0.01, ***p<0.001, **** p<0.0001 vs. siNC.
(**F**) Hypothetical diagram linking VRAC activity to the activity of the Cl^- sensitive WNK kinases and intracellular Cl^- homeostasis. The downstream protein kinases SPAK and OSR1 regulate activity of cation-chloride cotransporters NKCC1 and KCC1-4, which contribute to $[Cl^-]_i$ control.

Figure 6. LRRC8A knockdowns regulates mTORC2 signaling through WNK1-dependent mechanism

(**A**) Effect of WNK signaling inhibitor (WNK463, 0.1-3µM) on GBM1 proliferation. Proliferation rates were measured using the MTT assay and compared to vehicle control (0.1% DMSO). Data are the normalized mean values ± SD from 3 independent treatments.
(**B**) Effect of WNK1 knockdown on *Wnk1* mRNA levels. GBM1 cells were transfected with WNK1-specific siRNAs #5, #6, and #12 or the negative control siNC. Expression values were measured using qRT-PCR and normalized to *Rpl13a*. Data are the mean values ± SD. n=7 independent transfections. One-sample t-test with Bonferroni correction, *p<0.05, ****p<0.0001, vs. siNC.
(**C**) Effect of WNK1 knockdown on proliferation in GBM1 and GBM8. Cells were treated with WNK1-specific siRNAs (#5, #6, and #12) or the negative control siNC. Proliferation was measured using an MTT assay. Data are the normalized mean values ±SD from 7-9 independent transfections/cell line. One-sample t-test with Bonferroni correction, ****p<0.0001 vs. siNC.
(**D**) Diagram depicting hypothetical interaction between LRRC8A/VRAC, the Cl^--dependent WNK1, and mTORC2 signaling in GBM. VRAC promotes higher $[Cl^-]_i$ and formation of the signaling complex between the Cl^--bound WNK1 and mTORC2. mTORC2 activation promotes GBM proliferation via the downstream protein kinases AKT, SGK, and/or PKC.
(**E-G**) Western blot analysis of the effect of WNK1 downregulation on mTORC2 signaling in GBM1 cells, measured using AKT phosphorylation as a readout. Representative images and quantification of phospho-AKT (**E1-E2**), total AKT (**F1-F2**), and phospho/total AKT immunoreactivity ratio (**G**). GBM1 cells were transfected with WNK1-specific siRNAs (#5, #6, and #12) or the negative control siNC (n=6). As additional controls (n=3), GBM1 were treated with the AKT inhibitor MK-2206 (AKTi, 2.5 µM, 24 h) and the WNK inhibitor WNK463 (WNKi,

bioRxiv preprint doi: https://doi.org/10.1101/2025.02.02.636139; this version posted February 6, 2025. The copyright holder for this preprint (which was not certified by peer review) is the author/funder, who has granted bioRxiv a license to display the preprint in perpetuity. It is made available under aCC-BY-NC-ND 4.0 International license.

1µM, 24 h). NTF, non-transfected cells. Data are the mean values ±SD. One-way ANOVA with Dunnett's correction, ***p<0.001, **** p<0.0001 vs. siNC.

(**H-J**) Western blot analysis of the effect of LRRC8A downregulation on mTORC2 signaling in GBM, using AKT phosphorylation as a readout. Representative images and quantification of phospho-AKT (**H1-H2**), total AKT (**I1-I2**), and phospho/total AKT immunoreactivity ratio (**J**). GBM1 were treated with siA3, siA5, or siNC (n=7). Non-transfected cells (NTF) and cells treated with the PI3K inhibitor PI 828 (PI3Ki, 2.5 µM, 24 h) or the AKT inhibitor MK-2206 (AKTi, 2.5 µM, 24 hr) were included as additional controls (n=3-4). Data are the mean values ± SD. One-way ANOVA with Dunnett's correction, **p<0.01, ***p<0.001, ****p<0.0001 vs. siNC.

Figure 7. Effect of mTORC2-dependent signaling inhibition on GBM cell proliferation

(**A**) GBM1 cells were treated for 3 days with the inhibitors of AKT (AKTi; MK-2206, 2.5 µM), SGK (SGKi; GSK650394, 10 µM), PKC (PKCi; Gö6976, 3 µM), a combination of AKTi/SGKi/PKCi (Combo), or mTORC1/2 (mTORi; KU-0063794, 2.5 µM). The resulting effect on cell proliferation was measured using an MTT assay and compared to vehicle-treated cells (Veh; 0.167% DMSO). Data are the mean values ± SD from 6-9 independent treatments. One-way ANOVA with Bonferroni correction. ns, not significant, ****p<0.0001.

(**B**) The same pharmacological treatments as shown in panel A were evaluated for their effects on proliferation of GBM8 cells (n=6-9). One-way ANOVA with Bonferroni correction. ns, not significant, ****p<0.0001.

Figure 8. LRRC8A-containing VRAC regulates GBM proliferation through a WNK1/ mTORC2-dependent mechanism

Hypothetical model implicating the Cl^--dependent WNK1/mTORC2 signaling as the mechanistic link between LRRC8A expression, VRAC activity, and GBM proliferation. VRAC activity is proposed to sustain high $[Cl^-]_i$, promote formation of the complex between Cl^--bound WNK1 and mTORC2. The subsequent increase in mTORC2 activity promotes GBM proliferation through activation of homologous AKT and SGK.

bioRxiv preprint doi: https://doi.org/10.1101/2025.02.02.636139; this version posted February 6, 2025. The copyright holder for this preprint (which was not certified by peer review) is the author/funder, who has granted bioRxiv a license to display the preprint in perpetuity. It is made available under aCC-BY-NC-ND 4.0 International license.

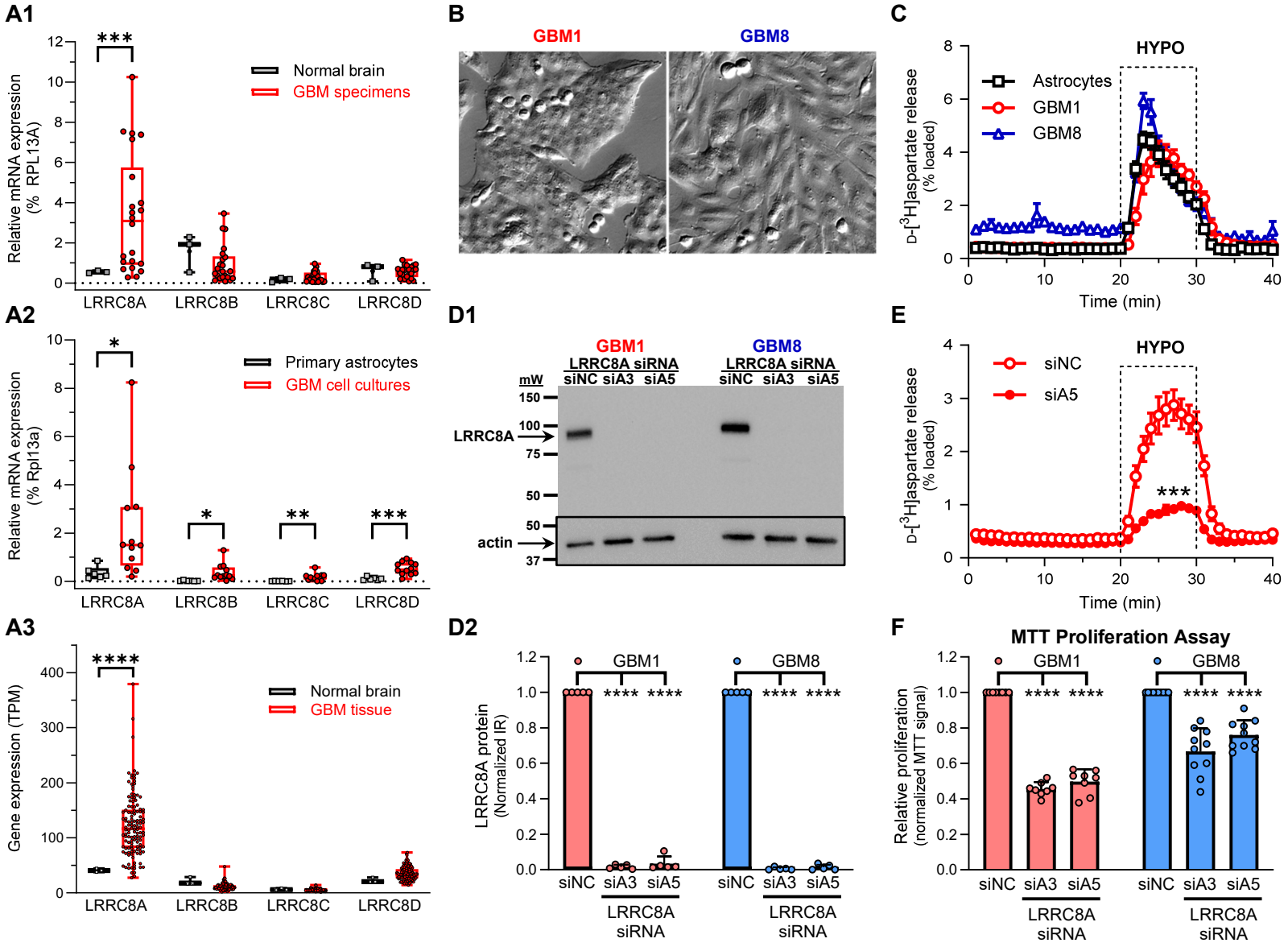

LRRC8A is upregulated in human GBM specimens and patient-derived GBM cultures and promotes cell proliferation

(**A1**) *Lrrc8* mRNA expression levels in surgically resected GBM tumor specimens (n=22) and healthy brain tissue (3 RNA medleys from 8 brains) measured using qRT-PCR and normalized to the housekeeping gene *Rpl13a*. ***p<0.001, GBM vs. normal brain.

(**A2**) Comparison of *Lrrc8* mRNA expression levels in patient derived GBM cell cultures (n=12) and primary human astrocytes (n=6). *p<0.05, **p<0.01, ***p<0.001, GBM vs. astrocytes.

(**A3**) In-silico analysis of RNA-seq data for the expression of *Lrrc8* isoforms in primary GBM (n=126) and healthy brain tissue (3 RNA medleys from 29 brains). GBM expression values were obtained from TCGA. Healthy brain tissue data were sourced from GEO repository, series GSE196695. ****p<0.0001, GBM vs. normal brain.

In A1-A3, data are presented as boxplots with individual values and compared with an unpaired t-test with Welch correction and Holm-Šídák adjustment.

(**B**) Representative images of the patient-derived GBM1 (*LEFT*) and GBM8 (*RIGHT*) cells. Images were acquired using Hoffman optics at identical 160× magnification.

(**C**) VRAC activity in GBM1, GBM8, and primary human astrocytes measured as swelling activated release of preloaded D-[^{3}H]aspartate. Cell swelling was induced by 30% reduction in medium osmolarity (HYPO). Mean values ±SEM from 4-6 independent experiments/cell line.

(**D1**) Representative western blot image probing downregulation of LRRC8A in GBM1 and GBM8 cells treated with the LRRC8A-specific siRNAs, siA3 and siA5, and compared to the negative control siRNA (siNC). Lower inset shows the same membrane re-probed for β-actin immunoreactivity.

(**D2**) Quantification of LRR8A expression in siRNA-treated GBM cultures. Mean values ±SD from 5 independent transfections/cell line. One-sample t-test with Bonferroni's correction. ****p<0.0001 vs siNC.

(**E**) Functional downregulation of VRAC activity in GBM1 cells treated with LRRC8A siRNA (siA5) and compared to siNC. Mean values ±SEM (n=5/condition). ***p<0.001 vs. siNC, t-test comparing integral D-[^{3}H]aspartate release values during hypotonic exposure.

(**F**) Effect of LRRC8A knockdown with the LRRC8A-specific siRNAs siA3 and siA5 on relative proliferation in GBM1 and GBM8 measured using the MTT assay. Mean values ±SD from 8-10 independent transfections. One-sample t-test with Bonferroni's correction, ****p<0.0001 vs. siNC.

bioRxiv preprint doi: https://doi.org/10.1101/2025.02.02.636139; this version posted February 6, 2025. The copyright holder for this preprint (which was not certified by peer review) is the author/funder, who has granted bioRxiv a license to display the preprint in perpetuity. It is made available under aCC-BY-NC-ND 4.0 International license.

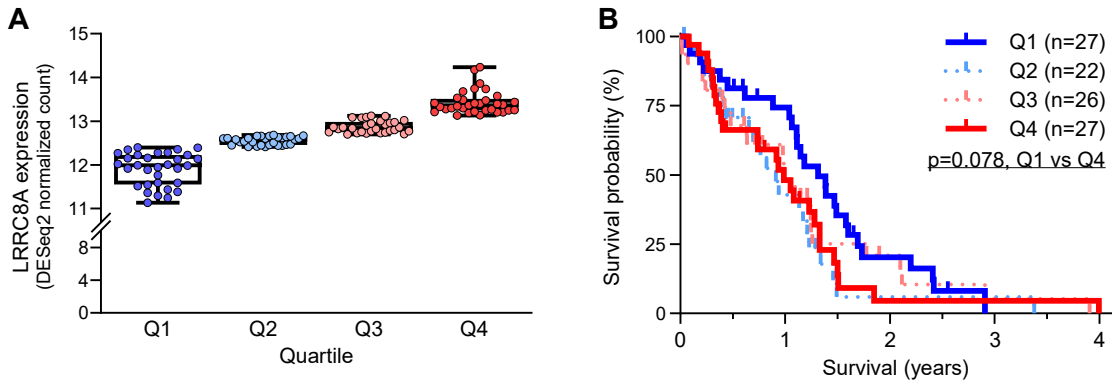

In-silico analysis of the relationship between *Lrrc8a* mRNA expression and life expectancy in GBM patients

(**A**) In-silico analysis of RNA-seq expression for *Lrrc8a* in primary GBM tissues (n=126) separated into quartiles. Data were sourced from TCGA and normalized using the DEseq2 variance-stabilizing transformation. Expression values presented as boxplots with individual values.

(**B**) Kaplan-Meier plot of survival rates for GBM patients grouped by tumor *Lrrc8a* expression quartile. Median survival was compared between the lowest (Q1; n=27) and highest (Q4; n=27) *Lrrc8a* expressers using the Gehan-Breslow-Wilcoxon test. p=0.078.

bioRxiv preprint doi: https://doi.org/10.1101/2025.02.02.636139; this version posted February 6, 2025. The copyright holder for this preprint (which was not certified by peer review) is the author/funder, who has granted bioRxiv a license to display the preprint in perpetuity. It is made available under aCC-BY-NC-ND 4.0 International license.

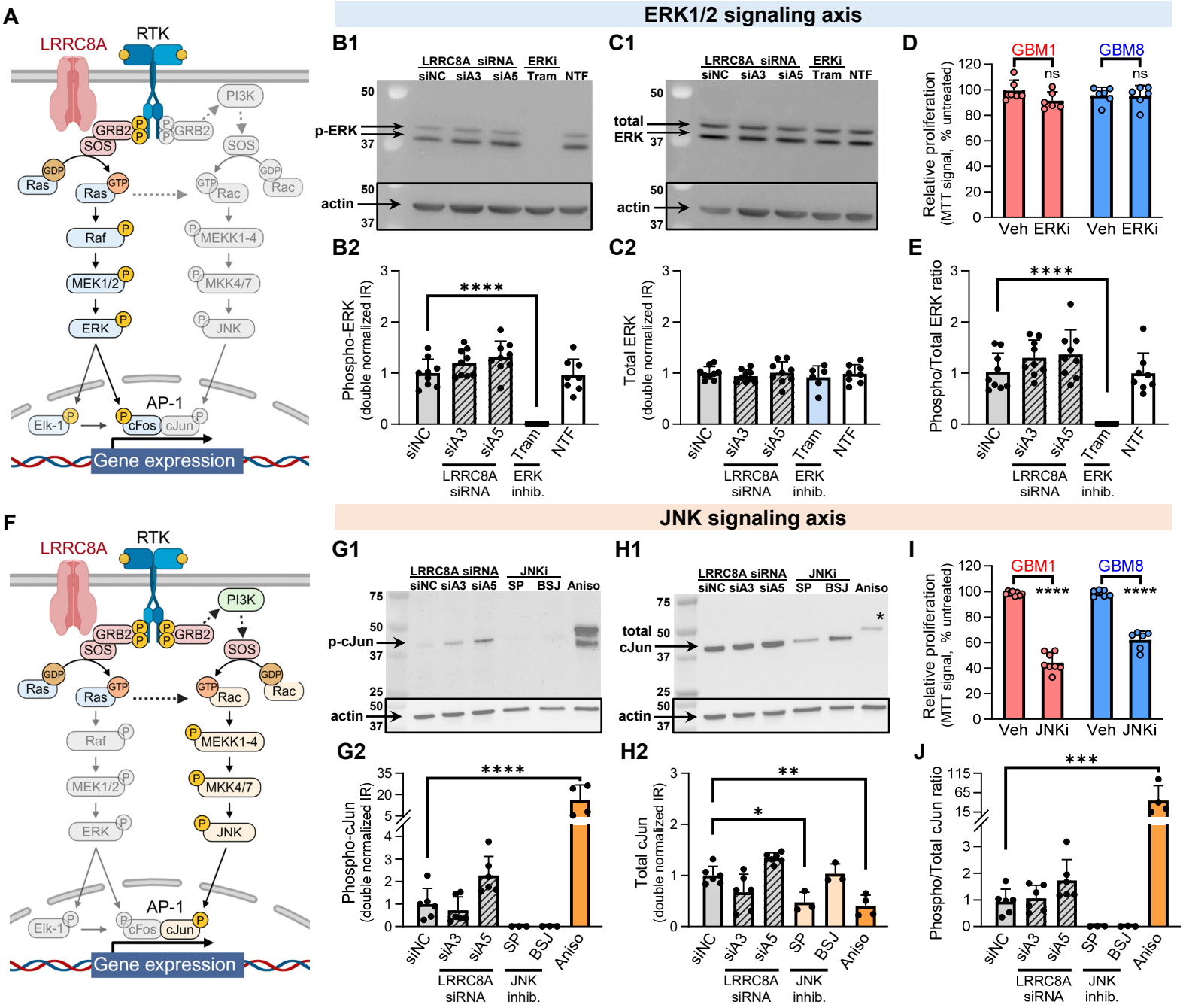

Analysis of functional interactions between LRRC8A and GRB2-dependent growth factor signaling pathways in GBM

(**A**) Diagram depicting receptor tyrosine kinase (RTK)-ERK1/2 signaling pathway and its putative interactions with LRRC8A. For abbreviations and further information see text.

(**B,C,E**) Western blot analysis of the effect of LRRC8A downregulation on ERK1/2 signaling in GBM1 cells. Representative images and quantification of phospho-ERK1/2 (**B1-B2**), total ERK1/2 (**C1-C2**), and phospho/total ERK1/2 immunoreactivity ratio (**E**). GBM1 cells were treated with the LRRC8A-specific siRNAs, siA3 and siA5, and compared to the negative control siNC (n=9). GBM1 cells treated with the ERK1/2 inhibitor Trametinib (Tram; 0.3 μM, 6-hr) and non-transfected cells (NTF) were included as additional controls (n=6-8). Data are the mean values ± SD. One-way ANOVA with Dunnett's correction, ****p<0.0001, trametinib vs siNC.

(**D**) Effect of the ERK1/2 signaling inhibitor U-0126 (ERKi; 10μM) on GBM1 and GBM8 proliferation as compared to vehicle control (Veh; 0.1% DMSO). Cell proliferation values were measured using the MTT assay and normalized to within-plate untreated cells (n=6/cell line). Data are the mean values ± SD. ns, not significant, unpaired t-test.

(**F**) Diagram depicting RTK-JNK signaling pathway and its putative interactions with LRRC8A. For abbreviations and further information see text.

(**G,H,J**) Western blot analysis of the effect of LRRC8A downregulation on JNK signaling in GBM1 cells using cJun phosphorylation as a readout. Representative images and quantification of phospho-cJun (**G1-G2**), total cJun (**H1-H2**), and phospho/total cJun immunoreactivity ratio (**J**) in GBM1 cells treated with the LRRC8A-specific siA3 and siA5 as compared to siNC. As controls, GBM1 were treated with the JNK inhibitor SP600125 (SP, 20μM, 24-hr), the MKK4/7 inhibitor BSJ-04-122 (BSJ, 5μM, 24-hr), or the JNK activator anisomycin (Aniso; 10μM, 2-hr). Data are the mean values ± SD from 6 siRNA experiments and 3-4 pharmacological controls. One-way ANOVA with Dunnett's correction, *p<0.05, **p<0.01, ***p<0.001, ****p<0.0001 vs. siNC.

(**I**) Effect of the JNK signaling inhibitor SP600125 (JNK-i, 20μM) on GBM1 and GBM8 proliferation. The MTT assay values were normalized to within-plate untreated cells and compared to the vehicle control (Veh; 0.1% DMSO). Data are the mean values ± SD (n=6-8/cell line). Unpaired t-test, ****p<0.0001 vs. Veh.

bioRxiv preprint doi: https://doi.org/10.1101/2025.02.02.636139; this version posted February 6, 2025. The copyright holder for this preprint (which was not certified by peer review) is the author/funder, who has granted bioRxiv a license to display the preprint in perpetuity. It is made available under aCC-BY-NC-ND 4.0 International license.

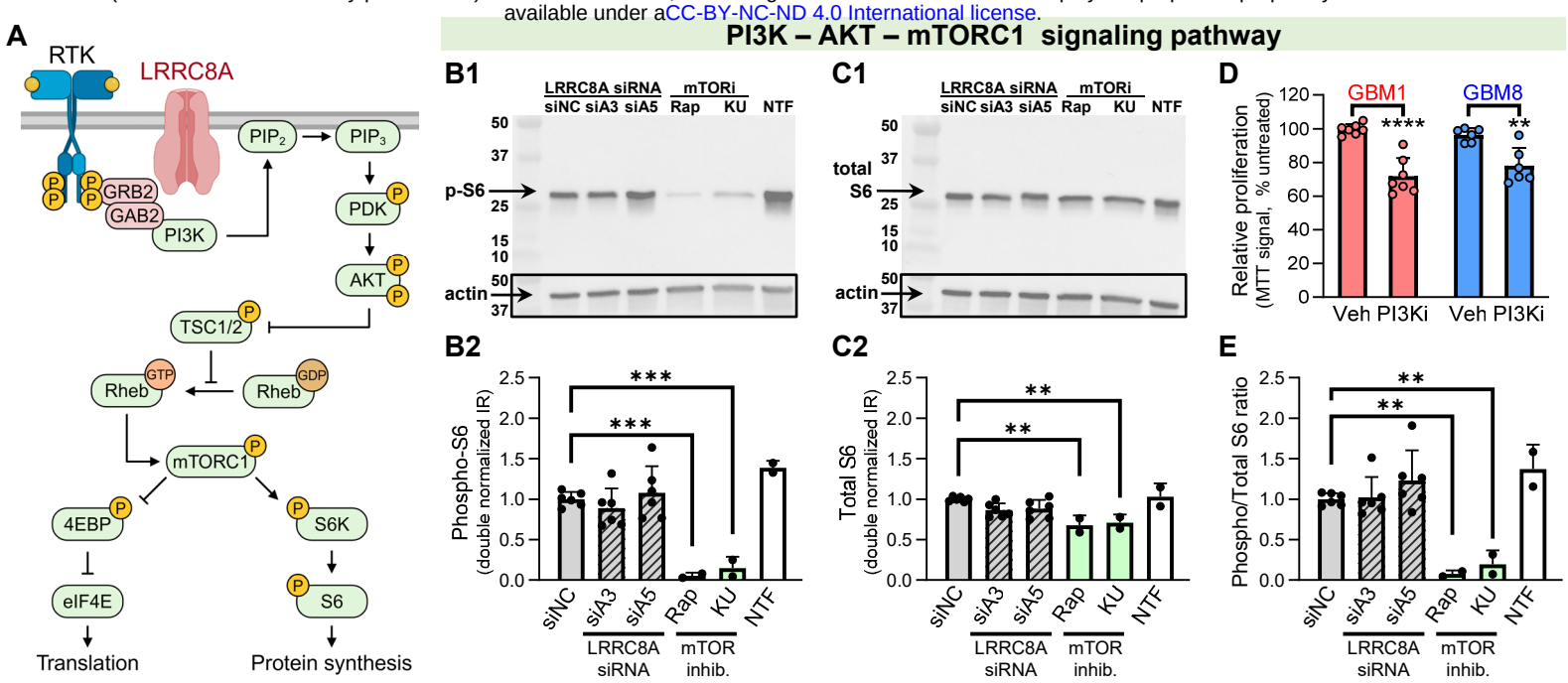

Analysis of functional interactions between LRRC8A and the GRB2-dependent PI3K/AKT/mTORC1 signaling axis in GBM

(**A**) Diagram depicting RTK-PI3K/AKT/mTORC1 signaling axis and its putative interactions with LRRC8A. For abbreviations and further information see text.

(**B,C,E**) Western blot analysis of the effect of LRRC8A downregulation on mTORC1 signaling in GBM, measuring S6 phosphorylation as a readout. Representative images and quantification of phospho-S6 (**B1-B2**), total S6 (**C1-C2**), and phospho/total S6 immunoreactivity ratio (**E**). GBM1 cells were treated with the LRRC8A-specific siRNAs, siA3 and siA5, or the negative control siNC. As controls, cells were treated with the mTORC1 inhibitor Rapamycin (Rap, 10nM, 48-hr), or the mTORC1/2 blocker KU-0063794 (KU, 2.5 μM, 48-hr). NTF, non-transfected cells. Data are the mean values ± SD from 6 siRNA transfections or 2-3 pharmacological controls. One-way ANOVA with Dunnett's correction, **p<0.01, ***p<0.001 vs. siNC.

(**E**) Effect of the PI3K signaling inhibitor PI 828 (PI3Ki, 2.5μM) on GBM1 and GBM8 proliferation. The MTT assay values were normalized to within-plate untreated cells and compared to the vehicle control (Veh; 0.1% DMSO). Data are the mean values ± SD (n=6-7/cell line). Unpaired t-test, **p<0.01, ****p<0.0001 vs. Veh.

bioRxiv preprint doi: https://doi.org/10.1101/2025.02.02.636139; this version posted February 6, 2025. The copyright holder for this preprint (which was not certified by peer review) is the author/funder, who has granted bioRxiv a license to display the preprint in perpetuity. It is made available under aCC-BY-NC-ND 4.0 International license.

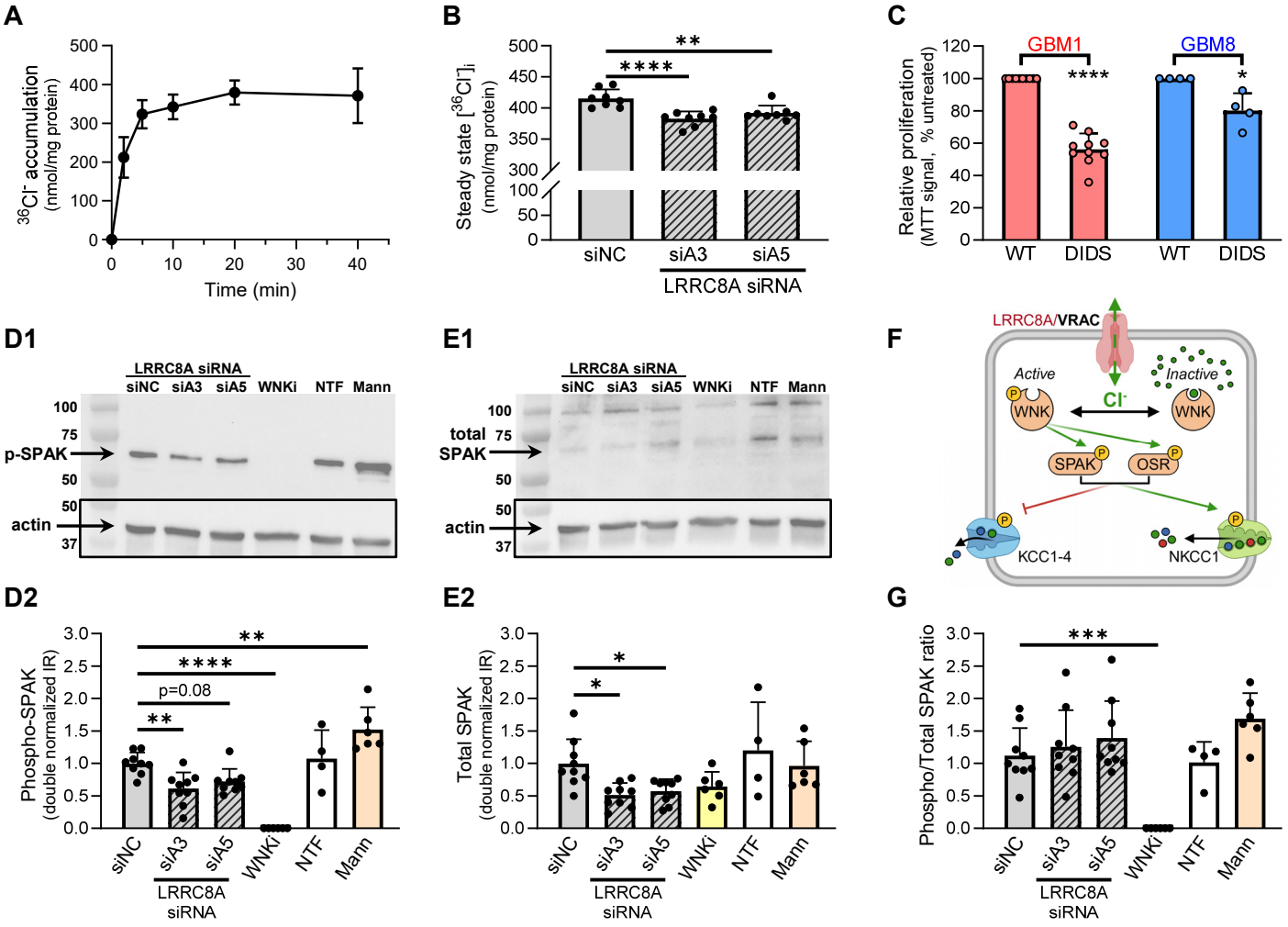

Effect of LRRC8A knockdown on $[Cl^-]_i$ and the Cl^--sensitive WNK signaling axis

(**A**) Kinetics of $^{36}Cl^-$ accumulation in GBM1 cells measured in a serum-containing cell culture medium. Data are the mean values ± SD of 4 independent assays.

(**B**) Effect of LRRC8A knockdown on a steady state $^{36}Cl^-$ accumulation in GBM1 cells. Cells were transfected with the LRRC8A-specific siRNAs, siA3 and siA5, or the negative control siNC. 96-h later, intracellular Cl^- levels were measured as steady state $^{36}Cl^-$ uptake. Data are the mean values ± SD from 8 independent transfections. One-way ANOVA with Dunnett's correction. **p<0.01, ****p<0.0001 vs. siNC.

(**C**) Effect of the putative VRAC blocker DIDS (500 µM) on GBM1 and GBM8 cell proliferation as compared to untreated cells (WT). Proliferation was quantified using an MTT assay and normalized to untreated cells on the same plate. Data are the mean ±SD. n=4-10/cell line. One-sample t-test. *p<0.05, ****p<0.0001 vs WT.

(**D,E,G**) Western blot analysis of the effect of LRRC8A downregulation on WNK signaling in GBM1, measured using SPAK phosphorylation as a readout. Representative images and quantification of phospho-SPAK (**D1-D2**), total SPAK (**E1-E2**), and phospho/total SPAK immunoreactivity ratio (**G**). GBM1 were treated with the LRRC8A-specific siA3 and siA5 or the negative control siNC (n=9). As controls, cells were treated with the WNK inhibitor WNK463 ('WNKi', 1µM, 24-hr) or hyperosmotic medium supplemented with 300 mM mannitol ('Mann', 1-hr treatment). NTF, non-transfected cells. n=4-6 for pharmacological controls. Data are the mean ±SD. One-way ANOVA with Dunnett's correction, *p<0.05, **p<0.01, ***p<0.001, **** p<0.0001 vs. siNC.

(**F**) Hypothetical diagram linking VRAC activity to the activity of the Cl^- sensitive WNK kinases and intracellular Cl^- homeostasis. The downstream protein kinases SPAK and OSR1 regulate activity of cation-chloride cotransporters NKCC1 and KCC1-4, which contribute to $[Cl^-]_i$ control.

bioRxiv preprint doi: https://doi.org/10.1101/2025.02.02.636139; this version posted February 6, 2025. The copyright holder for this preprint (which was not certified by peer review) is the author/funder, who has granted bioRxiv a license to display the preprint in perpetuity. It is made available under CC-BY-NC-ND 4.0 International license.

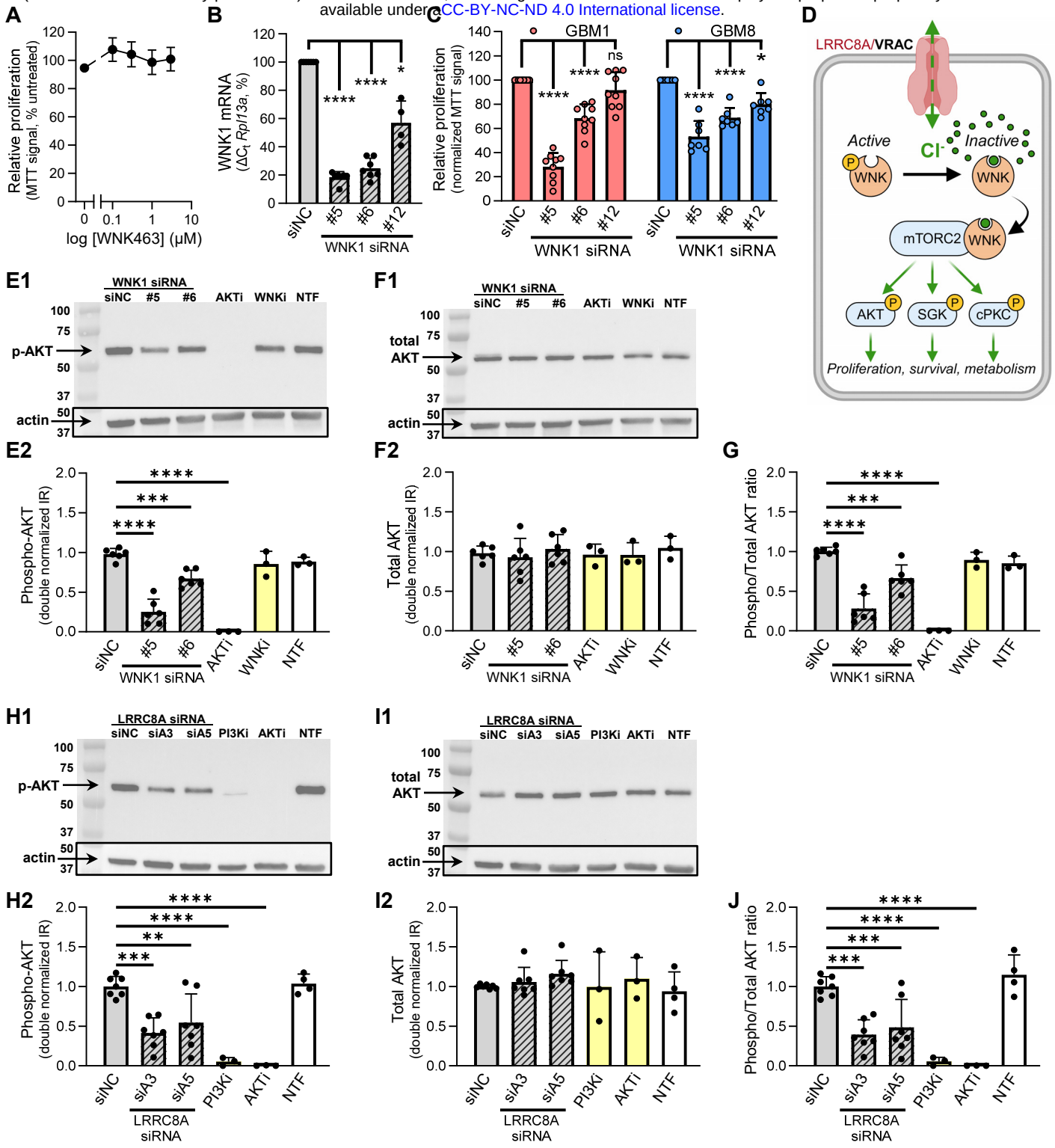

LRRC8A knockdowns regulates mTORC2 signaling through WNK1-dependent mechanism

(**A**) Effect of WNK signaling inhibitor (WNK463, 0.1-3μM) on GBM1 proliferation. Proliferation rates were measured using the MTT assay and compared to vehicle control (0.1% DMSO). Data are the normalized mean values ± SD from 3 independent treatments.

(**B**) Effect of WNK1 knockdown on *Wnk1* mRNA levels. GBM1 cells were transfected with WNK1-specific siRNAs #5, #6, and #12 or the negative control siNC. Expression values were measured using qRT-PCR and normalized to *Rpl13a*. Data are the mean values ± SD. n=7 independent transfections. One-sample t-test with Bonferroni correction, *p<0.05, ****p<0.0001, vs. siNC.

(**C**) Effect of WNK1 knockdown on proliferation in GBM1 and GBM8. Cells were treated with WNK1-specific siRNAs (#5, #6, and #12) or the negative control siNC. Proliferation was measured using an MTT assay. Data are the normalized mean values ±SD from 7-9 independent transfections/cell line. One-sample t-test with Bonferroni correction, ****p<0.0001 vs. siNC.

(**D**) Diagram depicting hypothetical interaction between LRRC8A/VRAC, the Cl^--dependent WNK1, and mTORC2 signaling in GBM. VRAC promotes higher $[Cl^-]_i$ and formation of the signaling complex between the Cl^--bound WNK1 and mTORC2. mTORC2 activation promotes GBM proliferation via the downstream protein kinases AKT, SGK, and/or PKC.

(**E-G**) Western blot analysis of the effect of WNK1 downregulation on mTORC2 signaling in GBM1 cells, measured using AKT phosphorylation as a readout. Representative images and quantification of phospho-AKT (**E1-E2**), total AKT (**F1-F2**), and phospho/total AKT immunoreactivity ratio (**G**). GBM1 cells were transfected with WNK1-specific siRNAs (#5, #6, and #12) or the negative control siNC (n=6). As additional controls (n=3), GBM1 were treated with the AKT inhibitor MK-2206 (AKTi, 2.5 μM, 24 h) and the WNK inhibitor WNK463 (WNKi, 1μM, 24 h). NTF, non-transfected cells. Data are the mean values ±SD. One-way ANOVA with Dunnett's correction, ***p<0.001, **** p<0.0001 vs. siNC.

(**H-J**) Western blot analysis of the effect of LRRC8A downregulation on mTORC2 signaling in GBM, using AKT phosphorylation as a readout. Representative images and quantification of phospho-AKT (**H1-H2**), total AKT (**I1-I2**), and phospho/total AKT immunoreactivity ratio (**J**). GBM1 were treated with siA3, siA5, or siNC (n=7). Non-transfected cells (NTF) and cells treated with the PI3K inhibitor PI 828 (PI3Ki, 2.5 μM, 24 h) or the AKT inhibitor MK-2206 (AKTi, 2.5 μM, 24 hr) were included as additional controls (n=3-4). Data are the mean values ± SD. One-way ANOVA with Dunnett's correction, **p<0.01, ***p<0.001, ****p<0.0001 vs. siNC.

bioRxiv preprint doi: https://doi.org/10.1101/2025.02.02.636139; this version posted February 6, 2025. The copyright holder for this preprint (which was not certified by peer review) is the author/funder, who has granted bioRxiv a license to display the preprint in perpetuity. It is made available under aCC-BY-NC-ND 4.0 International license.

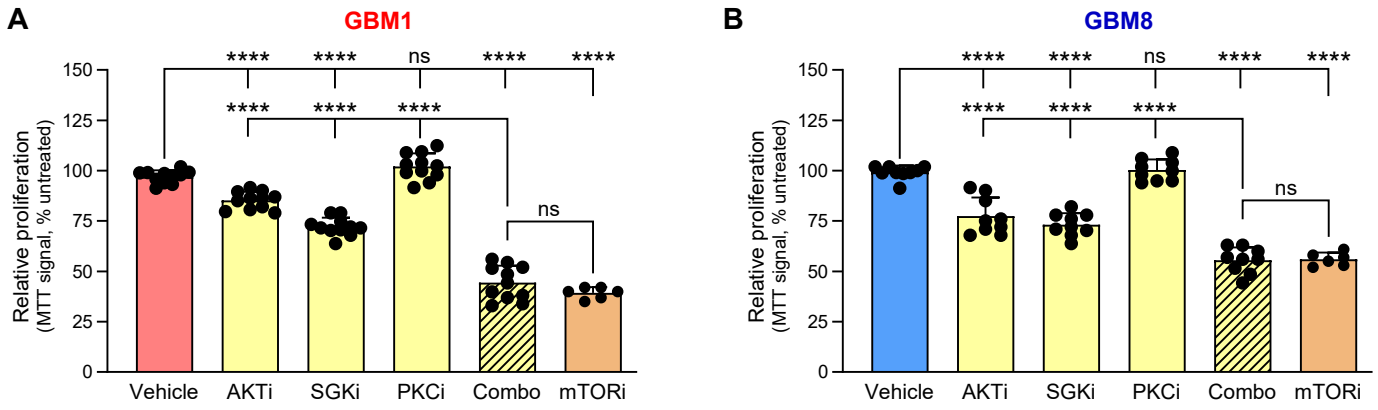

Effect of mTORC2-dependent signaling inhibition on GBM cell proliferation

(**A**) GBM1 cells were treated for 3 days with the inhibitors of AKT (AKTi; MK-2206, 2.5 μM), SGK (SGKi; GSK650394, 10 μM), PKC (PKCi; Gö6976, 3 μM), a combination of AKTi/SGKi/PKCi (Combo), or mTORC1/2 (mTORi; KU-0063794, 2.5 μM). The resulting effect on cell proliferation was measured using an MTT assay and compared to vehicle-treated cells (Veh; 0.167% DMSO). Data are the mean values ± SD from 6-9 independent treatments. One-way ANOVA with Bonferroni correction. ns, not significant, ****p<0.0001.

(**B**) The same pharmacological treatments as shown in panel A were evaluated for their effects on proliferation of GBM8 cells (n=6-9). One-way ANOVA with Bonferroni correction. ns, not significant, ****p<0.0001.

bioRxiv preprint doi: https://doi.org/10.1101/2025.02.03.636139; this version posted February 6, 2025. The copyright holder for this preprint (which was not certified by peer review) is the author/funder, who has granted bioRxiv a license to display the preprint in perpetuity. It is made available under aCC-BY-NC-ND 4.0 International license.

Figure 8 and Graphical Summary. Fidaleo, Bach *et al.*

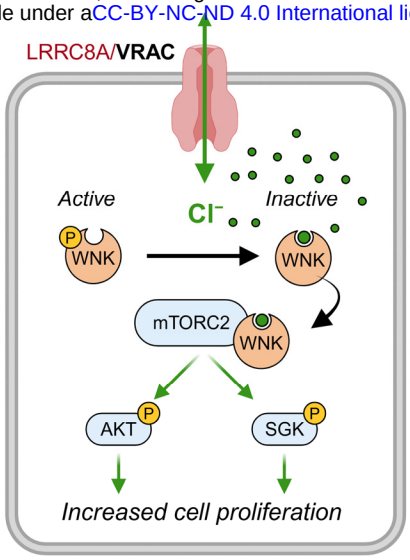

LRRC8A-containing VRAC regulates GBM proliferation through a WNK1/mTORC2-dependent mechanism

Hypothetical model implicating the Cl^--dependent WNK1/mTORC2 signaling as the mechanistic link between LRRC8A expression, VRAC activity, and GBM proliferation. VRAC activity is proposed to sustain high $[Cl^-]_i$, promote formation of the complex between Cl^--bound WNK1 and mTORC2. The subsequent increase in mTORC2 activity promotes GBM proliferation through activation of homologous AKT and SGK.